Applied Energy 404 (2026) 127154

Contents lists available at ScienceDirect

Applied Energy

journal homepage: www.elsevier.com/locate/apenergy

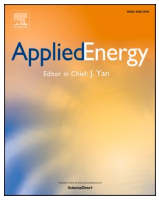

Numerical investigation on a high-temperature data center cooled by combined liquid-cooling and free-cooling - a comprehensive case study

Zi-Xing Wang, Ke Xue, Jun-Yu Chen, Nan Li, Wen-Quan Tao *

Key Laboratory of Thermo-Fluid Science & Engineering of MOE, Xi'an Jiaotong University, Xi'an, Shaanxi 710049, PR China

HIGHLIGHTS

- A liquid-cooling and free-cooling combined data center cooling scheme is proposed.
- The modified FRS condition achieves effective cooling of servers in the rack.
- The optimized AHU achieves a high ten-year average *COP* of 17.54.
- The studied DC achieves the ten-year average *PUE* and *COP* of 1.18 and 7.64.
- The *COP* of the free-cooling part is 2.2 times the *COP* of the water-cooling part.

ARTICLE INFO

Keywords:
Data center
Free cooling
Liquid cooling
Numerical simulation
Air handling unit

ABSTRACT

A high-performance cooling system is crucial for data center (DC) energy saving. This paper aims to model and analyze the cooling performance of a novel liquid-cooling and free-cooling combined cooling scheme proposed for high-temperature DC. The air-cooling and liquid-cooling combined servers (ALCS) and free-cooling air handling units (AHU) are combined in the DC. There is still no such study on the ALCS and AHU combined DC cooling performance at the complete DC system level. In this paper, the ANSYS Fluent and MATLAB SIMULINK are used to carry out the CFD simulation and the system-level simulation. For the studied DC in Xi'an, the effects of fans rotation speed (FRS) on IT room cooling performance are first investigated. When FRS is constant, under the inlet air/water temperature of 45 °C, the minimum FRS is 850 rad·s^{-1} to ensure the safe server operation, while the total rack fans power is 83.68 W. By adjusting the FRS in different ALCSs, a modified FRS working condition is obtained with better cooling performance and lower rack fans power (81.36 W). Then, the free-cooling performance of twelve AHU designs is tested. All AHU designs can meet the cooling requirement when the environment temperature is 15 °C, and the highest *COP* of AHU (COP_{AHU}) reaches 28. But when the environment temperature is as high as 40 °C, the highest COP_{AHU} is only 3.94. The optimized AHU design with the highest ten-year averaged COP_{AHU} of 17.54 for the studied DC in Xi'an is obtained. The studied DC exhibits effective cooling and energy consumption performance. For the ten-year period, the *PUE* and *COP* of DC are respectively 1.18 and 7.64. The *COP* of the free-cooling part has reached 2.2 times of the *COP* of the water-cooling part, which indicates that the application of AHU can effectively improve the cooling efficiency.

1. Introduction

With the development of digital technologies, the scale of data center (DC) is growing rapidly, and DC consume approximately 1 % - 1.5 % of global electricity according to the International Energy Agency [1]. The cooling system plays an important role in DC, which creates a stable and reliable operation environment for IT equipment. Adequate cooling for data centers is crucial to ensuring the reliability of IT equipment, preventing service interruption, and maintaining the stability of computing performance. The cooling system of DC consumes a large amount of electric power. The cooling system consumes about 32 % (the average value) of all electrical power in DC [2] for traditional air-cooled DC. The efficiency improvement of the cooling system in DC is crucial to save energy consumption in DC. The new energy-saving cooling technologies are required for the DC industry.

* Corresponding author.
E-mail address: wqtao@mail.xjtu.edu.cn (W.-Q. Tao).

https://doi.org/10.1016/j.apenergy.2025.127154
Received 9 August 2025; Received in revised form 31 October 2025; Accepted 23 November 2025
Available online 6 December 2025

Nomenclature

Abbreviations

AHU	Air handling unit
ALCS	Air-cooling and liquid-cooling combined server
CFD	Computational fluid dynamics
COP	Coefficient of performance
CPU	Central processing unit
CRAC	Computer room air conditioners
DC	Data center
FRS	Fans rotation speed
HDD	Hard disk drive
HVAC	Heating, ventilation, and air conditioning
IT	Internet technology
MPHE	Middle plate heat exchanger
PCB	Printed circuit board
PUE	Power usage effectiveness
WFR	Water flow rate

Parameters

a_1 to a_{10}	Constant parameters used in the chiller *COP* fitting formula
ρ_{air}	Air density

Variables

$A_{AHU\text{-}in}$	Total cross-section area of cold-side flow channels in AHU
COP_{AHU}	*COP* of AHU
$COP_{chiller}$	*COP* of the air-cooled chiller
$P_{AHU\text{-}fans}$	Fan power of AHU
$P_{additional}$	Power loss of power distribution and lighting
$P_{Pump\ \#1}$	Pumping power of the room-side pump
$P_{Pump\ \#2}$	Pumping power of the chiller-side pump
P_{server}	Power of servers
$P_{server\text{-}fans}$	Power of fans in servers
$P_{water\text{-}pump}$	Total power of pumps in the water-cooling system
Q_{AHU}	Heat dissipation rate of AHU
$Q_{chiller}$	Heat dissipation rate of the air-cooled chiller
$Q_{cold\text{-}plate}$	Total heat dissipation rate of cold plates
Q_{server}	Total heat dissipation power of servers
$q_{v\text{-}c}$, $q_{v\text{-}h}$	Cold/hot air volume flow of AHU
$T_{c\text{-}in}$, $T_{c\text{-}out}$	Inlet/outlet cold air temperature of AHU
$T_{h\text{-}in}$, $T_{h\text{-}out}$	Inlet/outlet hot air temperature of AHU
Δph, Δpc	Pressure drop of AHU hot-side and cold-side
$\eta_{AHU\text{-}fan}$	The total efficiency of AHU fans

1.1. Literature review

The legacy air-cooled DC generally uses conventional computer room air conditioners (CRAC) to dissipate the heat generated by the electronics [3,4]. For the traditional air-cooled DC, the air in the IT room is the heat-transfer medium between the server and the CRAC. The flow of air in the IT room can be named as the first cooling system [5]. The heat generated by the server is first transferred to the air by fan-forced convection in the server, then the heat is transferred to the liquid coolant by CRAC in the IT room, and finally, the heat is transferred to outdoors by the air-cooled chiller. The flow circulation of the liquid coolant can be named the second cooling system [5], while the CRAC is the middle equipment between the first cooling system and the second cooling system in the air-cooled DC.

For the first cooling system of traditional air-cooled DC, the poor thermal properties of air cause poor heat dissipation performance [6], and the server fans consume about 8 % of total DC power in legacy air-cooled DC, as reported by reference [2]. It requires significant fan power to form the airflow circulation in the room. In the past decade, various technologies have been studied and applied in DC to reduce the energy consumption of the first cooling system in DC, like temperature and airflow uniformity improvement [7], liquid-cooling technologies [8], and phase change materials cooling technology [9] etc. Among the new cooling technologies of the first cooling system, the liquid-cooling technology is becoming popular [10,11]. Compared with traditional air-cooling technology, liquid-cooling technology exhibits superior heat transfer efficiency due to liquids' higher heat capacities and heat transfer coefficients. The cold plate liquid cooling is the most widely utilized form of liquid cooling [12]. The microchannel cold plate achieves high heat dissipation ability and can meet the cooling requirements of modern CPU processors in DC [13]. Li et al. [14] studied 26 new microchannel cold plate designs by numerical simulation and experiment, and they obtained the optimized cold plate design with a high heat flux of 266.6 $W{\cdot}cm^{-2}$. Recently, the authors proposed a novel multilayered microchannel cold plate for commercial CPU-package cooling [15]. It is found that the multilayered microchannel cold plate can both achieve high cooling power and low pressure drop, and a modified stepped multi-layered microchannel cold plate design achieves a high CPU chip heat flux of 206.5 $W{\cdot}cm^{-2}$ while the pressure drop is only 523.5 Pa. For commercial CPU processor cooling, the cold plates are generally used by replacing the traditional air-cooled heat sink in DC, which changes a part of the cooling medium into the liquid coolant for the first cooling system of air-cooled DC. The liquid coolant is now the cooling medium of the CPU processors, while the cooling medium of the other components in the server is still air. Such a cold plate application approach is widely used in DC [16], in which the high-load chips/processors are cooled by liquid, and the low-load components are still cooled by fan-forced air. It is clear that the cold plate application in DC forms a hybrid air-cooling and liquid-cooling coupled scheme for the first cooling system. Both the air and liquid coolants should be further cooled by the second cooling system. In traditional air-cooled DC, the air is cooled by the liquid coolant in CRAC, while the coolant can be directly transferred to the middle plate heat exchanger (MPHE). The chiller is required to complete the heat transfer process from MPHE to outdoor air. The energy-saving performance evaluation of the cold plate should be considered under the complete heat transfer path from the indoor cold plate to the outdoor chiller.

For the second cooling system of DC, chillers are widely used to generate the chilled water for the cooling of the coolant circulation. The air-cooled chiller [17] and water-cooled chiller [18] are mostly used. The efficiency of the chiller is the main barrier to energy-saving of the second cooling system, as reported by reference [2], the HVAC accounts for about 24 % of the total power consumption of DC. Energy-saving of chiller in DC is a hot research direction. Recently, free-cooling has become popular in data centers, which is an energy-saving alternative to traditional chillers [19]. Free-cooling technologies adopt the natural climate (natural air or water) to cool DC [20]. By employing the natural climate, the utilization of CRAC and chiller plants can be reduced or potentially eliminated, which saves substantial cooling energy [21]. Khalaj et al. [4] utilized the air-side free-cooling economizer-based cooling system and achieved more than 80 % reduction of total cooling power for 42 DCs in major cities. Jia et al. [22] adopted a tap water-based free-cooling system and cooling tower free-cooling for a factory, and achieved an annual energy-saving ratio of 15.1 %. For most DC, natural air is the most readily available natural cold source. The natural air could be directly supplied to the IT room as the cooling medium, which is the direct air-side free-cooling technology [23]. Direct air-side free-cooling directly utilizes the cold air as the cooling medium, which has higher cooling efficiency and longer operation time. However, the direct utilization of natural air may affect the internal environment of

the IT room, Shehabi et al. [24] reported that the direct utilization of air causes nearly an order of magnitude increase in particle concentration in the IT room. The indirect air-side free-cooling is more widely applied in DC, which can be further enhanced by water evaporation [25]. The indirect air-side free-cooling eliminates a series of problems caused by external air entering the computer room and reduces operation and maintenance costs [21]. The core of indirect air-side free-cooling is the air-to-air heat exchanger [26], which is also named the air handling unit (AHU) [27]. The cold natural air and hot IT room return air are sent into the AHU and complete the heat transfer process. The IT room return air is cooled to the required temperature and is further sent back to the IT room. The utilized natural air is blown out of the heat exchanger. As a heat exchanger, a higher heat transfer rate and lower pressure drop (fan power) are the main improvement indicators of the AHU. In our previous work, the dimple structures [28] are adopted to enhance the heat transfer of AHU, and a new thermal design method of AHU is proposed to obtain the heat exchange rate and flow loss power based on computational fluid dynamics (CFD) results [29]. It can be observed that AHU achieves the heat transfer between the air-circulation in the IT room and the natural air, which can be regarded as an extremely simple second cooling system handling the cooling of indoor air-circulation. AHU achieves significant cooling energy savings since only the fan power is needed. However, an important obstacle to AHU application is the environment temperature. When the environment air is hot, the heat transfer temperature difference between the environment air and the indoor air is pretty small. Under extreme climates, the outdoor air temperature can be higher than the indoor air temperature. Free-cooling AHU is not suitable for traditional DC with high outdoor air temperature and low indoor air temperature. Conversely, free-cooling AHU is suitable for high-temperature DC, which has high indoor air temperature (even higher than the general outdoor air temperature). In 2011, ASHRAE expanded the range of allowable environmental conditions of IT equipment, and the new class A4 environment has an upper temperature bound of 45 °C [30]. Strutt [31] reported that when the environmental temperature of the IT room is increased from 27 °C to 35 °C, the free-cooling operation time can be improved from 80 % to 99 % in Europe. The most important issue of high-temperature DC application is the high-temperature tolerance of server components, especially the hard disk drive (HDD) and CPU [32]. For the high-temperature DC, the application of free-cooling is a promising energy-saving solution only if the operation temperature of the components can be ensured to be below their limit temperature. There are a few works that mention the detailed cooling scheme of the high-temperature DC. Zhang et al. [33] adopts a cooling tower to achieve the free-cooling of DC, the CRAC is retained for the studied DC. They found that when the IT room cooling temperature reaches 41 °C, it is possible to achieve 100 % free-cooling for all climate zones in the world. Iyengar et al. [34] combined the liquid-cooling server and free-cooling economizer for a high-temperature data center. The lab-level prototype allows the use of up to 45 °C liquid coolant to the rack, and the cooling scheme saves 30 % of cooling energy compared with the traditional air-cooled data center. Fan et al. [35] adopted a water-side economizer (cooling tower and water-to-water heat exchanger) as the free-cooling solution, they found that 100 % free-cooling can be achieved when the IT room air temperature is 42 °C. Liao et al. [36] studied the impact of operations parameters for a free-cooling indirect evaporative precooling system, they found that when the IT room return air is as high as 39 °C, an annual energy saving of 15.13 % is achieved.

1.2. Research gaps, novelty, and paper structure

As can be seen from the above literature review, the free-cooling studies in high-temperature DC are rare. The following points list the research gaps of free-cooling in high-temperature DC.

Research gaps:

1) Cooling towers are generally adopted as free-cooling equipment, but they require massive water consumption.
2) CRAC is still used for the present high-temperature DC studies. And the air flow and heat transfer performance in the IT room are generally not studied.
3) The system-level simulation with reliable methods is rare for the high-temperature data center. Then, the present results have relatively low engineering application value.

To fix the research gaps, the following point-to-point novel solutions are adopted in this paper:

1) The AHU is adopted for free-cooling in DC, which doesn't require water evaporation. The proposed DC cooling scheme has little water consumption.
2) The CRAC is not used. The air circulation in the IT room is cooled by the AHU independently. The air flow and heat transfer in the IT room are studied by CFD methods.
3) A system-level study is carried out, and the detailed DC cooling system simulation methods are adopted. The important DC information is obtained, which is sufficient for the initial design plan of the DC engineering application.

The cooling scheme for high-temperature DC proposed in this paper combines liquid-cooling and free-cooling. This paper is our second phase of work. In our first phase of work [37], the cooling performance of a 2 U air-cooling and liquid-cooling combined server (ALCS) under high air/water inlet temperature (45 °C) is studied. The original air-cooling heat sink of the CPU-package in the server is replaced by the water-cooled microchannel cold plate while the fans are reserved. We found that with the integration of water-cooled cold plates for high-load CPU processors, the fans can work under a low fans rotation speed (FRS) while the CPU chips, HDDs, memories, and power units can all operate under their limited temperature, although the air and water inlet temperature is as high as 45 °C. In this paper, the studied ALCS is adopted in the IT room. For the liquid-cooling part, cold plates are utilized for the cooling of high-load CPU processors, while the MPHE and air-cooled chiller are adopted to form the heat transfer path. For the free-cooling part, air-circulation forced by fans in ALCS and fans in AHU is adopted to cool the low-load components like HDDs, memories, and power units. The air-circulation in the IT room is cooled by AHU rather than the traditional CRAC. With the above cooling system design, a novel liquid-cooling and free-cooling combined high-temperature DC cooling system is proposed and studied at the whole DC level. The complete heat transfer path including the first and second cooling systems is considered in this paper. The combination of cold plates and AHU takes advantage of both liquid-cooling and free-cooling, which saves energy for the first and second cooling systems. There is still no such study on the cold plate and AHU combined DC cooling performance at the complete DC level, according to the author's knowledge. The DC cooling performance is investigated based on the historical environment temperature data in Xi'an.

The model and simulation method of the IT room CFD simulation, AHU, and water-cooling system are given in **Section 2**. The performance of the DC cooling system is given and discussed in **Section 3**. The conclusions are given in **Section 4**.

2. Method

The schematic diagram of the DC cooling system studied in this work is given in Fig. 1. It consists of three parts: AHU, IT room, and water-cooling system. The servers installed in the rack are the ALCS studied in our previous work [37]. The CPU-packages in the ALCS are cooled by the water-cooled microchannel cold plates. And the other components in the ALCS are cooled by the fan-forced air. The fans in the ALCSs drive the airflow from the cold aisle to the hot aisle in the IT room. The hot aisle is

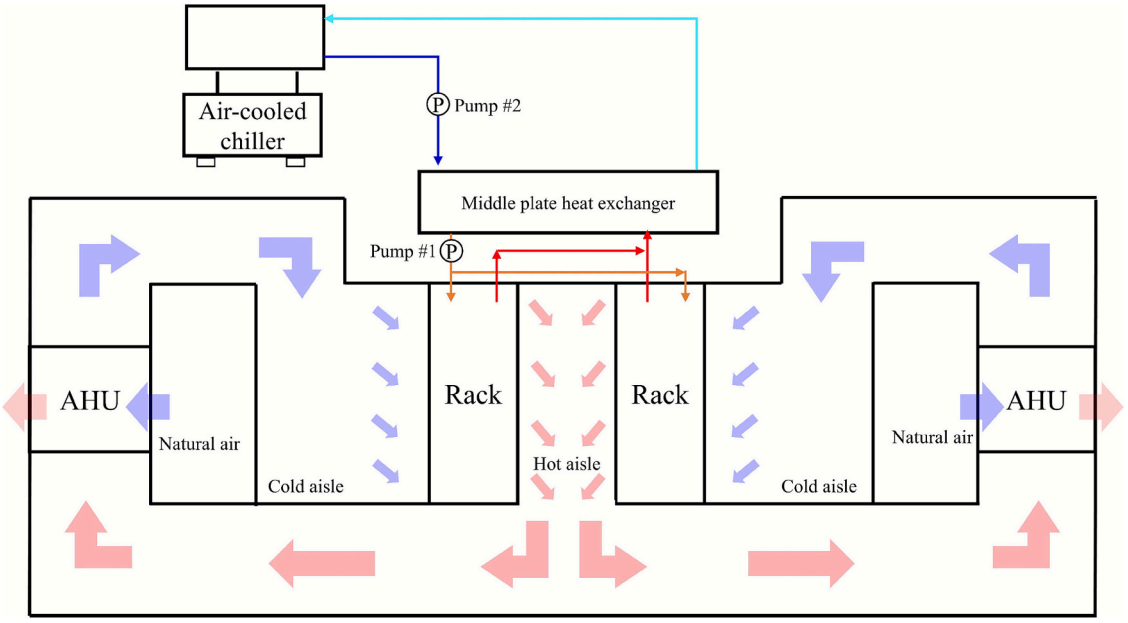

Fig. 1. The liquid-cooling and free-cooling combined DC cooling scheme.

enclosed, and the hot air in the hot aisle flows through the raised floor and then is cooled by the AHU, as shown in Fig. 1. The cooled air is circulated back to the IT room after its temperature is reduced to the required temperature by the AHU. Two rows of racks form the hot and cold aisles in the IT room, and Fig. 1 gives the cross-section of the two rows of racks. As for the water-cooling system in DC, the water pipe system is installed in the IT room, and the room-side pump (pump #1) drives the water circulation between ALCSs and the MPHE, as shown in Fig. 1. The air-cooled chiller and chiller-side pump (pump #2) form the chilling water circulation. In the DC, the main heat generated by CPU-packages is transferred to outdoor air step by step through the cold plate, MPHE, and air-cooled chiller. The main heat generated by other low-load components (HDDs, memories, power units, and mother PCB boards) is transferred to the outdoor air by air-circulation in the IT room and AHU.

The IT room, AHU, and water-cooling system are all modeled in this paper. The proposed cooling system consists of multi-scale components, and it is impossible to perform a complete three-dimensional CFD simulation for the whole DC. Thus, the simplified simulation method is adopted for the AHU and water-cooling system. As shown in Fig. 1, the DC cooling system can be separated into three parts (AHU, IT room, and water-cooling system), and different simulation models are developed for the three parts. The three-dimensional CFD model is adopted for the airflow and heat transfer in the IT room. The zero-dimensional models are developed for the AHU and water-cooled system. The air flow and heat transfer results of the IT room are first obtained from the CFD results of the IT room. Then the outlet air flow rate and temperature of the IT room are used in the simulation of the AHU model, and the required AHU fans' performance is obtained. The server outlet water temperature and flow rates of the ALCSs in the IT room are used in the water-cooling system model, and the energy consumption results of the water-cooling system are obtained. Finally, the overall cooling and energy consumption of the whole DC is summarized. The three-dimensional CFD simulation of the IT room air-circulation is accomplished by ANSYS Fluent, which is widely adopted in the air flow and heat transfer process in DC. The detailed air flow and heat transfer performance of air-circulation can be obtained by Fluent compared with other simulation tools like 6SigmaET and Simcenter Flotherm [37]. The CFD results of the IT room and AHU are extracted and adopted in the whole DC system simulation. The DC system simulation is finished using MATLAB SIMULINK. The advantage of this software lies in its mature basic simulation module and its editability feature. The detailed CFD simulation method and zero-dimensional system simulation models will be introduced in the following subsections.

2.1. Simulation method of air-circulation in the IT room

The air flow and cooling performance of air-circulation in the server room is obtained by CFD simulation. The following assumptions are adopted:

1. The air is treated as incompressible Newtonian fluid with constant physical properties. The solid regions also adopt constant physical properties.
2. The convection forced by fans dominates the air flow pattern, and the effects of gravity, irradiance, and natural convection are ignored.
3. The fan forced air flow in the IT room is turbulent flow.
4. The heat dissipation power is treated as constant and uniform heat sources in the energy equations for all heating components in the IT room.

Considering the periodic and symmetry characteristics of geometric structures, a typical unit of the IT room consisting of one rack is modeled for CFD simulation of air flow and heat transfer in the IT room, which is shown in Fig. 2. The IT room consists of ALCSs, rack, cold aisle, hot aisle, and underfloor air channel as shown in Fig. 2(a) and Fig. 2(b). Half of the hot aisle is modeled, and the middle cross-section of the hot aisle is treated as a symmetry boundary. The cooling air supplied by the AHU flows into the cold aisle through the air channel at the top of the room. Baffles are added to the inlet surface of the rack as shown in Fig. 2(c), and the cooling air flows into ALCSs through the inlet surfaces of the servers. The exhaust air flows through the hot aisle and underfloor air channel and exits at the outlet surface. There is a sharp turn in geometry between the hot aisle and the underfloor channel. Although the sharp turn may cause the reversed flow and airflow stagnation in the underfloor channel, the underfloor channel has a large height of 700 mm, and the airflow stagnation has little influence on the air exhausting performance of the underfloor channel. The exhaust air is further transferred to the inlet of the AHU and is cooled to the required temperature by the outdoor air.

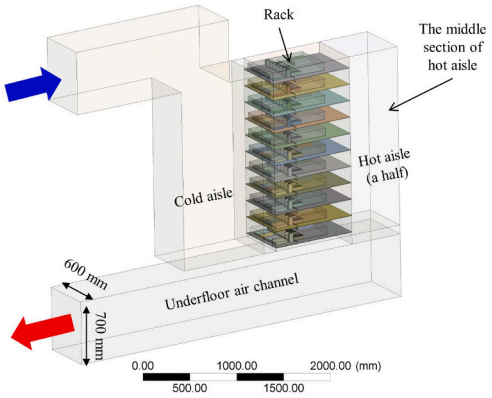

(a) The typical unit of IT room (iso-view)

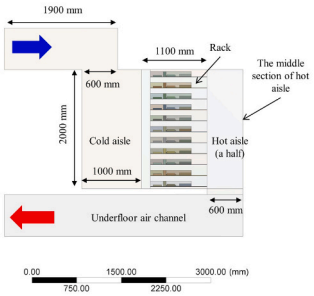

(b) The typical unit of IT room (side-view)

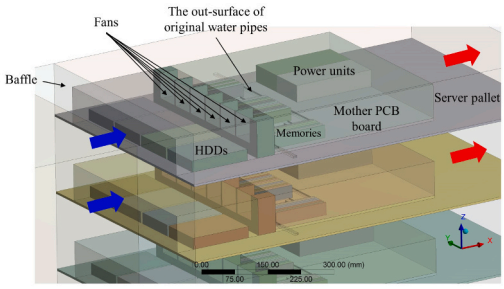

(c) The ALCS in the rack

Fig. 2. IT room geometry model. (a) The typical unit of IT room (isoview). (b) The typical unit of IT room (side-view). (c) The ALCS in the rack.

As shown in Fig. 2, eleven ALCSs are installed in one rack. The cooling performance of ALCS under different air/water inlet conditions has been comprehensively studied in our previous paper [37]. In the room-level study in this paper, the ALCSs are simplified by eliminating the domains of the water pipes, cold plates, and CPU-packages, which means the water-cooling part is not detailly simulated. However, the effects of the water-cooling parts are considered by applying the heat-flux boundary for the interface surfaces of the water-cooling parts and the servers. The fans in the ALCS are direct current axial fans with controllable FRS, and the FRS is controlled by the pulse width modulation method through the fans' controllers. For the ALCS, the simulation results under the same cooling conditions are adopted in this paper. The reason for adopting such simplified ALCS is the limitation of computational resources. In our previous work, the grid-independent result of ALCS was obtained under a mesh cell number of 119 million [37]. There are eleven ALCSs in the rack, as shown in Fig. 2. It requires billions of mesh cells to achieve the CFD simulation if all the structure of ALCSs is retained, which is difficult to carry out. To solve this problem and carry out the CFD simulation under an acceptable mesh cell number, the original water-cooling part of ALCS is removed. But the heat flux at the interface surfaces of the water-cooling part and other regions in the ALCS is reserved, the uniform heat flux boundary condition is adopted, and the heat flux value is based on the CFD simulation results of our previous work. Take the single server condition for example, Fig. 3 shows the above ALCS model simplification method and the comparison results of the simplification method and the original complete simulation results. As shown in Fig. 3(a) and Fig. 3(b), the original ALCS includes the liquid-cooling regions (water pipes, cold plates, and CPU-packages), which are removed in the simplified ALCS in this paper. In addition to simplifying the water-cooling part, the turbulence model and mesh generation method are adjusted in this paper to further reduce the mesh cell number. The SST k-ω model is adopted in the previous work, which requires that the y^+ value near the wall does not exceed 5. It makes a low cell height of the first layer mesh and the dense near-wall mesh, which causes a large mesh cell number. The turbulence model adopted in this paper is the Realizable k-ε model, which has been widely adopted in room-level air flow and cooling simulation [38]. The scalable wall function is adopted to solve the flow in the viscous sublayer. Then the dense mesh is not required in this work, and the total mesh number can be greatly reduced. Fig. 3(c) shows the generated mesh of the simplified ALCS in this paper. The unstructured mesh is adopted, and the mesh cell number is only 11.8 million. The other simulation methods, including the velocity-pressure coupling method, and the material physical parameters, are not changed. As for the prediction accuracy of the simplified ALCS, Fig. 3(d) shows the comparison of the simulation results obtained by the simulation method adopted in this paper and the original simulation results in our previous work [37]. It is clear that the air flow rate and the temperature of the server outlet air under different FRS are completely consistent between the simplified ALCS and the complete ALCS. The maximum relative deviation is only 0.23 %, which proves the reliability of the simplified ALCS simulation method adopted in this paper.

The boundary condition of the IT room is given in Fig. 4. The pressure inlet and constant inlet temperature are adopted for the inlet surface of the IT room. The gage pressure of the pressure inlet is set to 0 Pa, and the constant inlet air temperature is set to 45 °C. The pressure outlet with 0 Pa of the gage pressure is adopted for the outlet surface of the IT room. There are eleven ALCSs and sixty-six small fans in the IT room model. All fan regions are set as "3D Fan Zone" and the fan curve data from the manufacturer is adopted. The air flow in the IT room is forced by the fans in ALCSs. Thus, the pressure inlet condition is adopted for the inlet surface of the IT room. The side surfaces of the cold aisle, hot aisle, underfloor channel, air supply channel, and the middle cross-section of the hot aisle all adopt the symmetry boundary condition. These surfaces are the simplified boundary sections obtained through geometric symmetry, which cannot be treated as wall boundaries. The interface walls between the fluid regions and solid regions all adopt the thermal-coupled no-slip wall. The adiabatic wall is adopted for all side walls. The uniform heat source is adopted for HDDs, memories, power units, and the mother PCB board to simulate the heating effect of components.

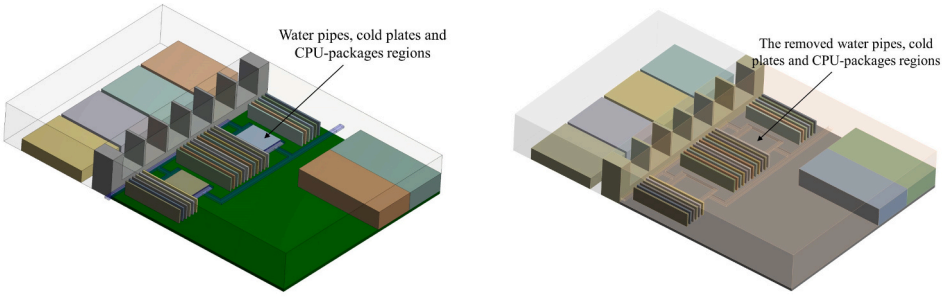

(a) The ALCS model in our previous work (b) The simplified ALCS model in this paper

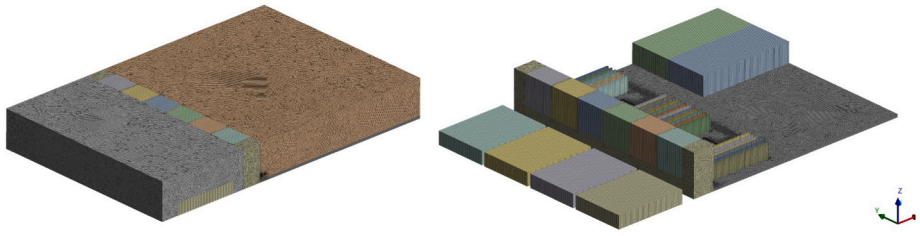

(c) The mesh of simplified ALCS (with a cell number of 11.8 million)

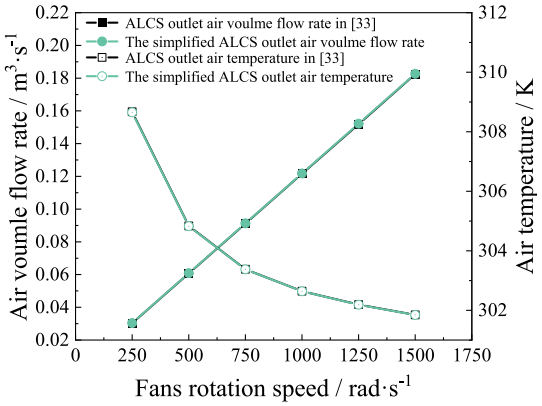

(d) The comparison of simplified ALCS in this paper and the original ALCS in [37] (water volume flow rate is 0.24L·min^{-1})

Fig. 3. The simplified ALCS and the comparison results between the simplified ALCS and the original ALCS. (a) The ALCS model in our previous work. (b) The simplified ALCS model in this paper. (c) The mesh of simplified ALCS (with a cell number of 11.8 million). (d) The comparison of simplified ALCS in this paper and the original ALCS in [37] (water volume flow rate is 0.24 L·min^{-1}).

For the studied DC case in this paper, the heat generation rates of the CPU processor, HDD, memory, power unit, and server PCB board are respectively 280 W, 14 W, 7 W, 20.2 W, and 80 W. The detailed ALCS simulation method, including the "3D fan zone" setting method, can be found in [37].

To validate the above simulation method of the air flow in the IT room, a comparison between the numerical method in this paper and the experiment data from reference [38] is given in Fig. 5. An IT room is modeled based on the geometry data from reference [38], as shown in Fig. 5(a). The air flow results are obtained based on the numerical method adopted in this paper, and Fig. 5(b) to Fig. 5(e) gives the comparison of area-averaged velocity at the inlet surfaces of servers between the numerical results and experimental data. The server air inlet velocity pattern of the numerical result agrees well with the experimental data. The maximum relative deviation is 5.25 % and the average relative deviation is 2.05 %. The model validation results indicate that the numerical method adopted in this paper for air flow in the IT room is accurate and reliable.

The grid-independent result of the IT room CFD simulation is given in Fig. 6(a) with an inlet air temperature of 300 K and all fans' FRS of 1000 rad·s^{-1}. The maximum temperature of HDDs and power units, the total pressure of outlet air, and the volume flow rate of outlet air are not changed with the increase of mesh cell number when the mesh cell number is larger than 223 million. Considering the consumption of computing resources and the reliability of simulation results, the IT room mesh with a 223 million mesh cell number is adopted for all IT room CFD simulation cases in this paper. The local mesh view is given in Fig. 6(b). The hexahedral mesh is generated in the rectangular region, and the tetrahedral mesh is generated in the unrectangular region.

The CFD simulation results of the IT room are coupled with the zero-dimensional models of the AHU and the water-cooling system. The coupling method is introduced in the following subsections.

2.2. *The model of AHU*

AHU is adopted for the cooling of the IT room outlet hot air by the natural cold air, as shown in Fig. 1. Twelve types of AHU heat exchangers (including the basic plate types and dimple-enhanced plate types) in our previous work [27,29] are adopted in this paper. The heat exchangers are enhanced by spherical crown dimples and elliptic cylindrical dimples with different dimple heights. The twelve AHU heat exchangers, including the basic flat plate AHU, are respectively named: "H12-basic", "H12R10h2", "H12R10h3", "H12R10h4", "H10-basic", "H10R10h2", "H10R10h3", "H10R10h4", "H7.5-basic", "H7.5R10h2", "H7.5R10h3", and "H7.5R10h4". The detailed geometry information on the twelve heat exchangers is given in reference [27]. The area-averaged

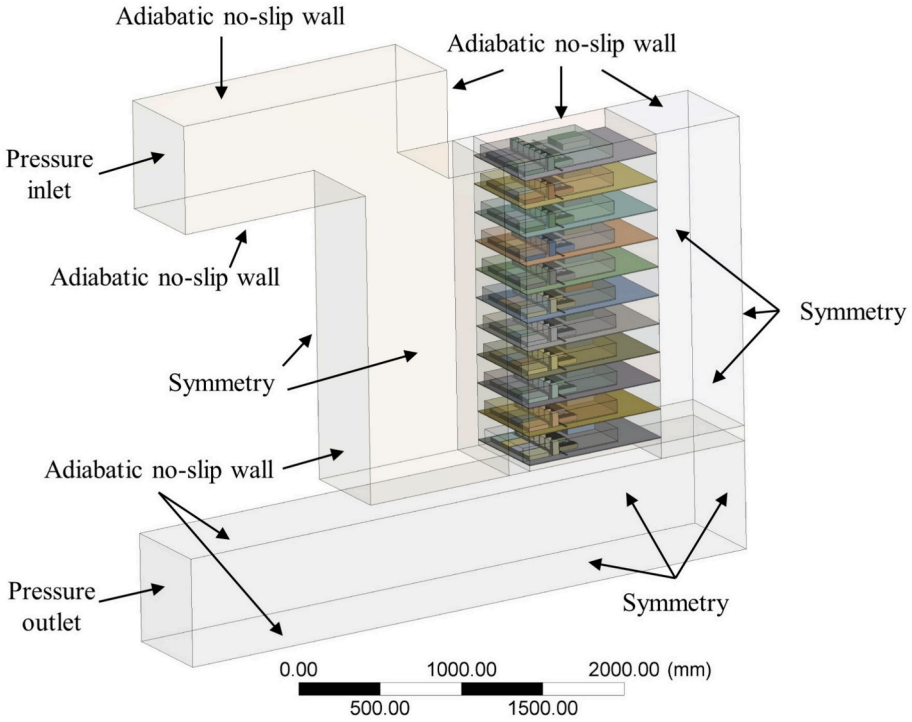

Fig. 4. The boundary condition of the IT room.

heat transfer coefficient and pressure drop data obtained in the references [27,29] are used and fitted by polynomial functions, which are given in **Appendix. A.** The area-averaged heat transfer coefficient and pressure drop fitting formulas are all reliable, with a high fitting R-square over 0.99. It is worth emphasizing that each type of AHU heat exchanger has a limited volume flow rate range to ensure the prediction accuracy of fitting formulas. The working condition of the AHU heat exchanger is based on the IT room's working condition. The CFD results of the air flow and heat transfer in the IT room are required before calculating the cooling performance of the AHU heat exchanger under different environment temperatures.

The AHU model consists of the core heat exchanger and two fans on the hot air side and the cold air side, as shown in Fig. 7(a). The core heat exchanger of AHU is an air-to-air heat exchanger as mentioned above. The fans in AHU are variable frequency drive fans with variable air volume flow rate. The air flow rates in cold side and hot side of AHU are both limited based on AHU heat exchanger type, and the flow rate limit regions are given in **Appendix. A**. The hot-air volume flow rate of AHU is constant in this paper based on the IT room condition. And the cold-air volume flow rate of AHU is changed by cold-side fan based on the environment air temperature.

The hot-air volume flow rate $q_{\text{v-h}}$, hot-air inlet temperature $T_{\text{h-in}}$, and hot-air outlet temperature $T_{\text{h-out}}$ are obtained from the IT room simulation results under identical server working conditions. When the AHU heat exchanger type is set, the pressure drop of hot air in AHU can be calculated by:

$$\Delta p_{\text{h}} = f_{\Delta p}(q_{\text{v-h}}) \tag{1}$$

where, Δp_{h} is the hot air pressure drop of AHU, Pa; $f_{\Delta \text{p}}(q_{\text{v-h}})$ is the fitting formula of pressure drop of the chosen AHU heat exchanger type; the formulas of $f_{\Delta \text{p}}(q_{\text{v-h}})$ are given in **Appendix. A**.

The hot air is forced by hot-side fans in AHU to overcome the flow resistance of the hot-side channels. The fan power of the hot-side fan in one AHU can be calculated by:

$$P_{\text{AHU-hot-fan}} = \frac{q_{\text{v-h}} \Delta p_{\text{h}}}{\eta_{\text{AHU-fan}}} \tag{2}$$

where, $P_{\text{AHU-hot-fan}}$ is the fan power of the hot-side fan in one AHU heat exchanger, W. $\eta_{\text{AHU-fan}}$ is the total efficiency of AHU fans, assumed as 0.75, which is feasible for commercial axial fans.

The cold-side fan forces the environment air to flow through the cold-side channels in the AHU heat exchanger to cool the hot-side air to meet the required air inlet temperature of the IT room. The cold-air inlet temperature $T_{\text{c-in}}$ is treated as the same as the environment temperature. Then the cold-side air flow rate $q_{\text{v-c}}$ needs to be obtained, which can be calculated by the following equations:

$$Q = \frac{1}{\frac{1}{h_{\text{h}}(q_{\text{v-h}})A} + \frac{1}{h_{\text{c}}(q_{\text{v-c}})A}} \Delta T \tag{3}$$

$$Q = q_{\text{v-h}} \rho c_{\text{p}} (T_{\text{h-in}} - T_{\text{h-out}}) \tag{4}$$

where, Q is the total heat transfer rate of one AHU heat exchanger, W; $h_{\text{h}}(q_{\text{v-h}})$ and $h_{\text{c}}(q_{\text{v-c}})$ are respectively the area-averaged heat transfer coefficient of the hot-side channel and cold-side channel in AHU, $\text{W}\cdot\text{m}^{-2}\cdot\text{K}^{-1}$. For the set AHU heat exchanger type, $h_{\text{h}}(q_{\text{v-h}})$ and $h_{\text{c}}(q_{\text{v-c}})$ have same fitting formulas given in **Appendix. A**. ΔT is the logarithmic mean temperature difference of hot air and cold air/ K. A is the projected heat transfer area of AHU heat exchanger, m^2; ρ is the density of air, 1.1785 $\text{kg}\cdot\text{m}^{-3}$; c_{p} is the thermal capacity of air, 1020 $\text{J}\cdot\text{kg}^{-1}\cdot\text{K}^{-1}$.

When the IT room condition is set, $q_{\text{v-h}}$, $T_{\text{h-in}}$, and $T_{\text{h-out}}$ can be obtained from the CFD simulation results of the IT room, then Q is obtained by **Eq. (4)**. With the environment temperature ($T_{\text{c-in}}$) and Q for the set AHU exchanger type, the cold-air volume flow rate $q_{\text{v-c}}$ is obtained by a searching method.

The detailed AHU heat transfer rate calculation method is given in our previous work [29]. Fig. 7(b) shows the $q_{\text{v-c}}$ searching process. Based on the known IT room CFD results, the hot side parameters of AHU ($q_{\text{v-h}}$, $T_{\text{h-in}}$, $T_{\text{h-out}}$) are known. The environment temperature is also known as the input data. Based on these known parameters, $q_{\text{v-c}}$ can be calculated. For the AHU heat exchanger, $q_{\text{v-c}}$ must be in the limited range. Thus, the minimum $q_{\text{v-c}}$ is first tested to judge if the required AHU heat transfer rate can be ensured under the minimum $q_{\text{v-c}}$, as shown in Fig. 7(b). If the calculated AHU heat transfer rate is larger than the required AHU heat

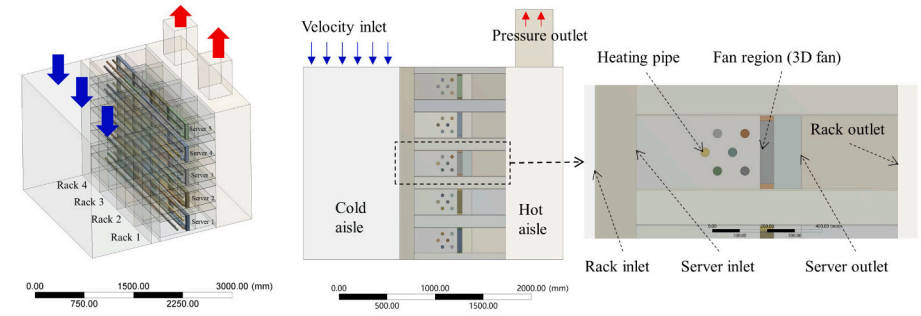

(a) The built room model with servers used for model validation.

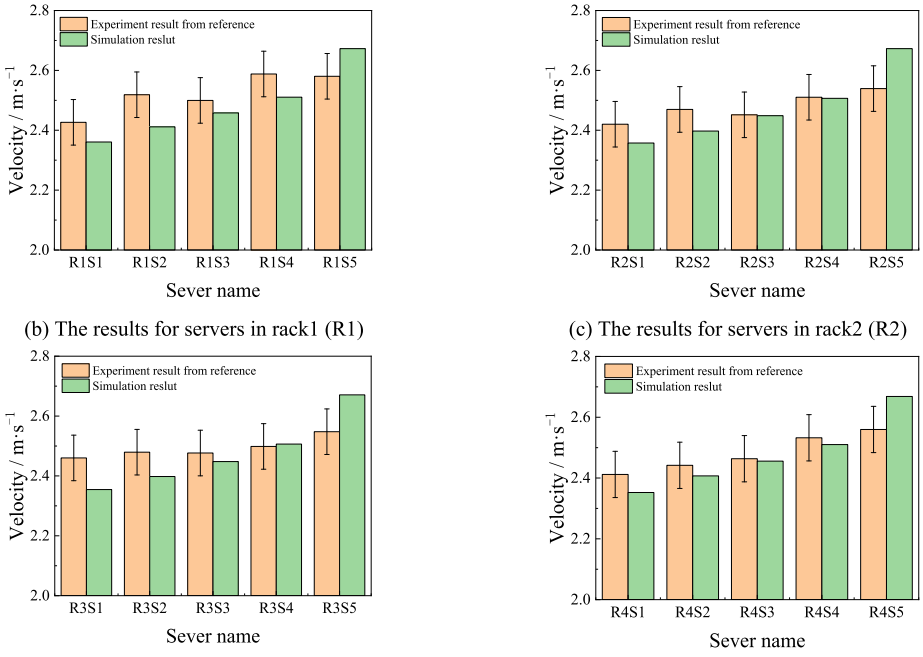

(b) The results for servers in rack1 (R1)

(c) The results for servers in rack2 (R2)

(d) The results for servers in rack3 (R3)

(e) The results for servers in rack4 (R4)

Fig. 5. The comparison of the area-averaged velocity at the inlet surface of the servers between the experiment results and the simulation results [37]. (a) The built room model with servers used for model validation. (b) The results for servers in rack1 (R1). (c) The results for servers in rack2 (R2). (d) The results for servers in rack3 (R3). (e) The results for servers in rack4 (R4).

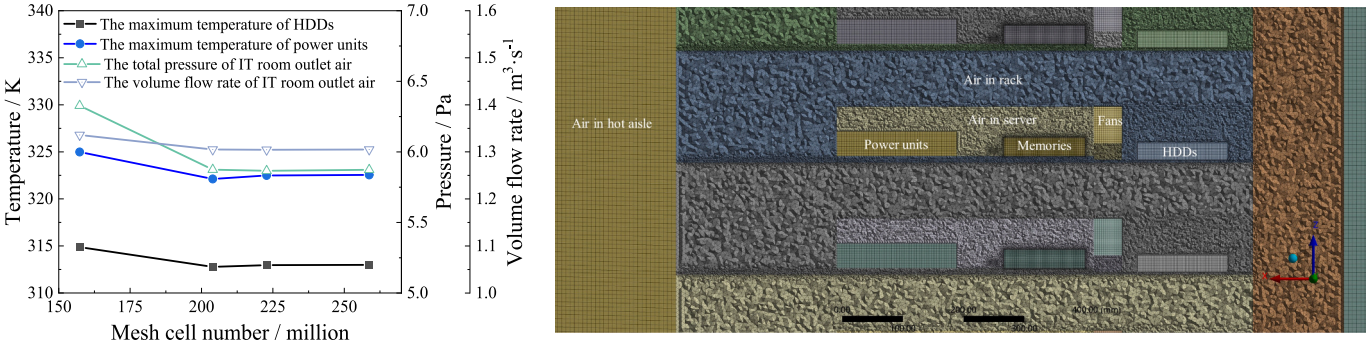

(a) Grid-independent test result

(b) Local mesh view

Fig. 6. The grid-independent result and the local mesh view of the chosen mesh. (a) Grid-independent test result. (b) Local mesh view.

transfer rate, the $q_{v\text{-}c}$ is set as the minimum volume flow rate. If the calculated AHU heat transfer rate is smaller than the required heat transfer rate, $q_{v\text{-}c}$ is increased with a small step until the calculated AHU heat transfer rate is larger than the required heat transfer rate. If the maximum $q_{v\text{-}c}$ can't meet the requirement of heat transfer rate, this type of AHU heat exchanger is set as an inapplicable AHU for the studied DC.

As introduced in **subsection 2.1**, the outlet surface of the underfloor channel of the IT room has a height and width of 700 mm and 600 mm. Thus, the AHU heat exchanger adopted in this paper has a height and length of 700 mm, and it can be installed at the downstream of the underfloor channel outlet surface. The width of the AHU heat exchanger is limited to 600 mm. Based on the above AHU geometry parameters

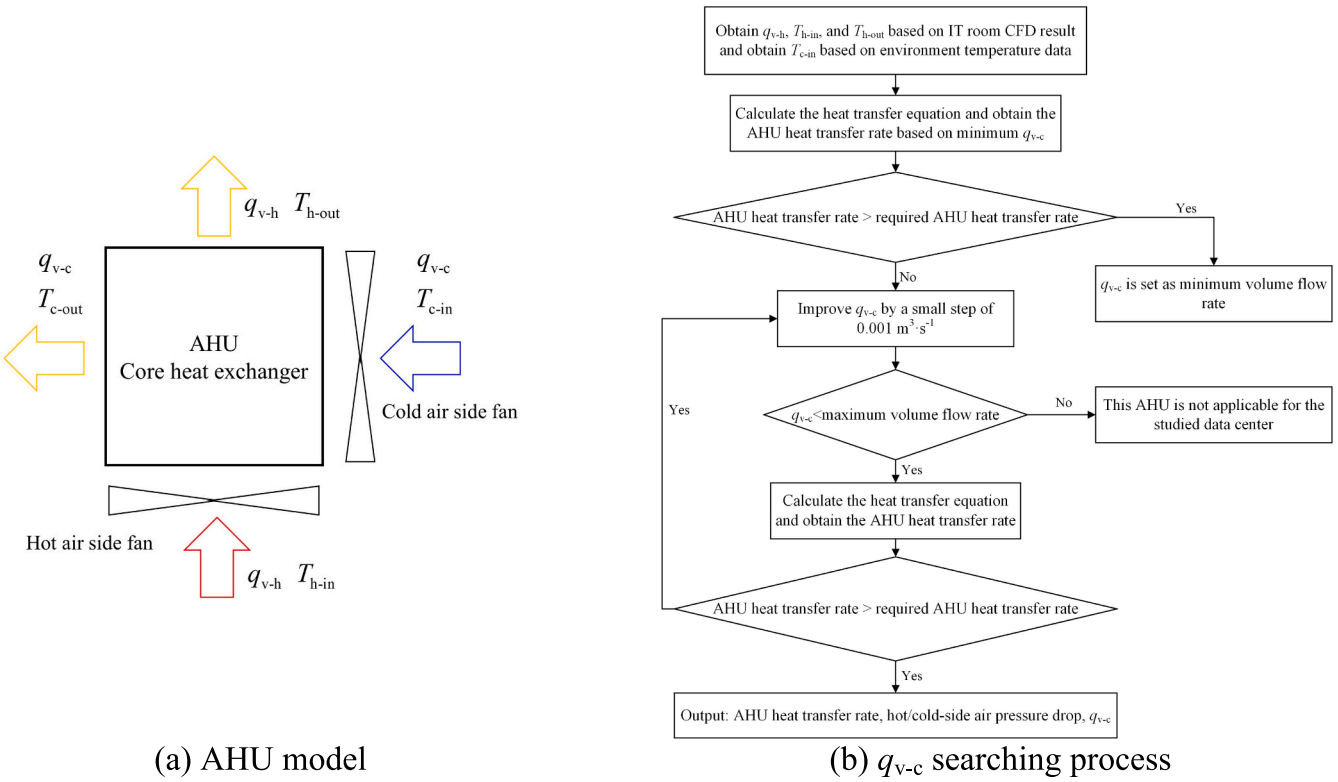

Fig. 7. The AHU model and $q_{v\text{-}c}$ calculation process for an identical AHU. (a) AHU model. (b) $q_{v\text{-}c}$ searching process.

limitation, the detailed heat exchanger parameters for all AHU heat exchanger can be obtained: the length × height × width of "H12" series AHU is 700 mm × 700 mm × 583.35 mm and the total channel number of "H12" series AHU is 48; the length × height × width of "H10" series AHU is 700 mm × 700 mm × 588.85 mm and the total channel number of "H10" series AHU is 58; the length × height × width of "H7.5" series AHU is 700 mm × 700 mm × 596.85 mm and the total channel number of "H7.5" series AHU is 78.

When $q_{v\text{-}c}$ is obtained with the above process for identical IT room working conditions and AHU heat exchanger type, the cold-side fan power for one AHU is calculated by:

$$P_{\text{AHU-fan-cold}} = \frac{q_{v\text{-}c}\Delta p_c + \frac{1}{2}(q_{v\text{-}c}\rho) \times \left(\frac{q_{v\text{-}c}}{A_{\text{AHU-in}}}\right)^2}{\eta_{\text{AHU-fan}}} \tag{5}$$

where, $P_{\text{AHU-fan-cold}}$ is the cold-side fan power of one AHU, W; Δp_c is the cold-side pressure drop of AHU, Pa, which is calculated by the fitting formulas given in **Appendix. A**. $A_{\text{AHU-in}}$ is the total cross-section area of cold-side flow channels of AHU heat exchanger, m^2. For "H12", "H10", and "H7.5" series AHU heat exchangers, the $A_{\text{AHU-in}}$ are respectively 0.2016 m^2, 0.203 m^2, and 0.20475 m^2. $\eta_{\text{AHU-fan}}$ is the total efficiency of AHU fans, 0.75.

To meet the cooling requirement of the IT room, the total fan power for one AHU heat exchanger is calculated by:

$$P_{\text{AHU-fans}} = P_{\text{AHU-fan-hot}} + P_{\text{AHU-fan-cold}} \tag{6}$$

The coefficient of performance (*COP*) of AHU is defined by:

$$COP_{\text{AHU}} = \frac{Q_{\text{AHU}}}{P_{\text{AHU-fans}}} \tag{7}$$

where, COP_{AHU} is the *COP* of the AHU heat exchanger.

2.3. The model of the water-cooling system

The water-cooling system in this paper can be divided into the indoor part and the outdoor part. The indoor part is a cooling water pipe system, which supplies the cooling water for the servers in the IT room. The water pipe system consists of the inlet main pipe, the inlet manifold pipe in the rack, the outlet manifold pipe in the rack, and the outlet main pipe. In this paper, a typical water pipe system consists of ten parallel racks, the sample of a typical water pipe system is given in Fig. 8. It can be seen that the inlet main pipe is arranged at the top of the racks, after the cooling water is evenly transferred into the racks, the outlet main pipe is also arranged at the top of the racks. In order to control the uniform distribution of cooling water flow, flow controllers are integrated at the inlet of the servers. The pressure drop of a typical water pipe system is required for the water pumping power calculation. To obtain the pressure of the water pipe system, the following assumptions are adopted: 1, assuming the water is uniformly distributed; 2, all pipes and joints are square and smooth. When the total water volume flow rate is known based on the cold plate working conditions, using the above assumptions, the pressure drop of the typical pipe system in Fig. 8 can be calculated. The frictional pressure drop and local pressure drop for long pipes and local connection structures in the pipe system are calculated by the equations from the handbook of hydraulic resistance [39,40]. The detailed calculation method and results for a case are given in the **Appendix. B**. It is worth emphasizing that the pipe is assumed as square pipe, and the pressure drop equations summarized for square pipes and square joints are adopted. Although, the circular pipes are typically adopted in the engineering application. The pressure drop calculation results of square pipes and circular pipes with the same hydraulic diameter have little difference, according to the authors' knowledge. Thus, the square pipes/joints pressure drop calculation results is acceptable for this system-level simulation work.

The outdoor part of the water-cooling system consists of water pumps, an MPHE, and an air-cooled water chiller, as shown in Fig. 9. There are two cooling water circulations in the Fig., one is driven by

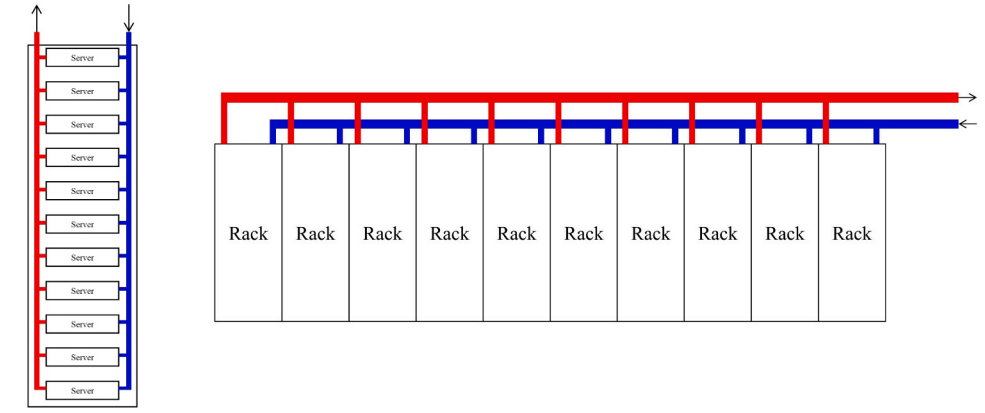

(a) Pipes in rack (b) Pipes outside the racks (the room level)

Fig. 8. The typical water pipe system in the IT room. (a) Pipes in rack. (b) Pipes outside the racks (the room level).

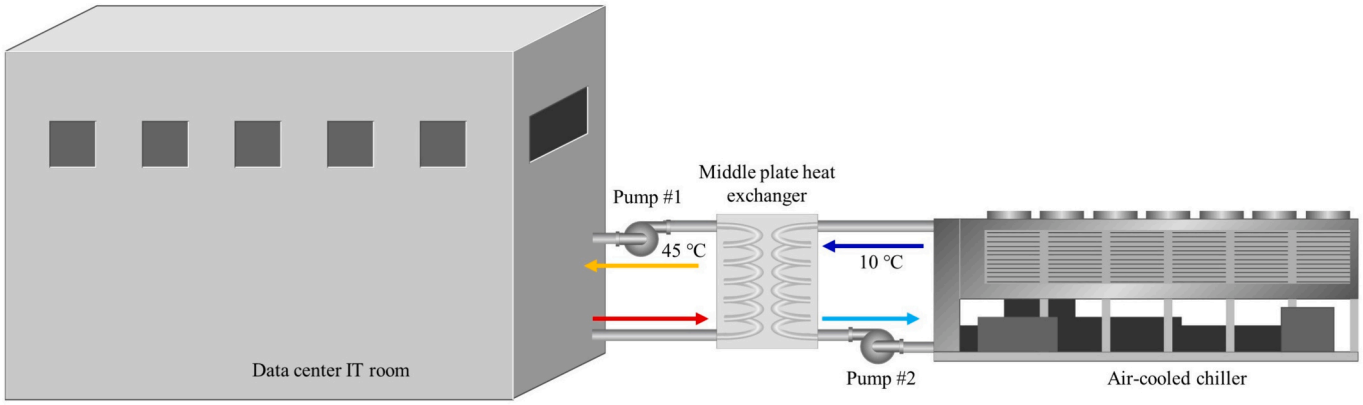

Fig. 9. The outdoor part of the water-cooling system.

pump #1 and another is driven by pump #2. The hot water exiting from the IT room is cooled to 45 °C by MPHE. The air-cooled chiller supplies the 10 °C chilled water to the MPHE.

The variable-frequency centrifugal water pump with controllable water flow rate is adopted. When the water volume flow rate and pressure drop are known, the pumping power of pumps can be calculated by **Eq. (8)** and **Eq. (9)**.

$$P_{\text{Pump\#1}} = \frac{q_{\text{v-room}}(\Delta p_{\text{room}} + \Delta p_{\text{PHE-hot}})}{\eta_{\text{Pump}}} \tag{8}$$

$$P_{\text{Pump\#2}} = \frac{q_{\text{v-chiller}}\Delta p_{\text{PHE-chiller}}}{\eta_{\text{Pump}}} \tag{9}$$

where $P_{\text{pump \#1}}$ and $P_{\text{pump \#2}}$ are respectively the pumping power of pump #1 and pump #2 in Fig. 9, W; $q_{\text{v-room}}$ and $q_{\text{v-chiller}}$ are respectively the water volume flow rate of IT room side and chiller side pipe system, $m^3 \cdot s^{-1}$; Δp_{room} is the water pressure drop of indoor part water pipe system, Pa; $\Delta p_{\text{PHE-hot}}$ is the hot water pressure drop of MPHE, Pa; $\Delta p_{\text{PHE-chiller}}$ is the cold water pressure drop of MPHE, Pa; The two side pressure drop of MPHE is obtained by heat exchanger design software. η_{pump} is the efficiency of water pumps, 0.75.

The MPHE is designed by HTRI Xchanger Suite [41] under the required working conditions. The chosen MPHE design result is given in **Appendix. C**, in which the detailed working condition of MPHE is given. As for the air-cooled chiller, the widely utilized multivariate polynomial model is adopted in this paper to obtain the power consumption of the chiller [42,43]. The *COP* of the air-cooled chiller can be calculated by the following equation.

$$COP_{\text{chiller}} = a_1 + a_2 \cdot Q_{\text{cooling}} + a_3 \cdot T_{\text{eo}} + a_4 \cdot T_{\text{a}} + a_5 \cdot Q_{\text{cooling}}^2 + a_6 \cdot T_{\text{eo}}^2 + a_7 \cdot T_{\text{a}}^2 + a_8 \cdot Q_{\text{cooling}} \cdot T_{\text{eo}} + a_9 \cdot Q_{\text{cooling}} \cdot T_{\text{a}} + a_{10} \cdot T_{\text{eo}} \cdot T_{\text{a}} \tag{10}$$

where, COP_{chiller} is the *COP* of air-cooled chiller, which is defined by the cooling capacity divided by electric power; a_1 to a_{10} are the constant coefficients; T_{eo} is the return water temperature of chiller, which is the temperature of chilled water transported into MPHE, 10 °C. T_{a} is the environment air temperature, °C. Q_{cooling} the cooling capacity, kW.

The air-cooled screw chiller with R134a as refrigerating fluid is adopted. The chiller is modeled by the experimental data of our laboratory. One thousand experiment data points are used for the formula fitting of COP_{chiller}, which is given in the Supplementary Material 1. Table 1 gives the value of constant coefficients obtained by COP_{chiller} fitting, and Fig. 10 gives the relative error between the fitted value and experimental data. It can be seen that the relative error between the fitting results and the experimental data is less than 10 % for most chiller working conditions, which shows the reliability of the COP_{chiller} fitting results used in this paper. Also, the COP_{chiller} versus Q_{cooling} curves for

Table 1
The parameter values of COP_{chiller}.

Parameter	value	Parameter	value
a_1	−2.93493	a_6	−0.00891
a_2	0.01208	a_7	0.00182
a_3	0.43867	a_8	7.81349×10^{-4}
a_4	0.2507	a_9	-5.40143×10^{-4}
a_5	-4.56714×10^{-6}	a_{10}	−0.02117

different T_a and constant T_{eo} are given in Fig.E-1.

The numerical result of the ALCS is adopted in this paper for the model of the water-cooling system. The optimized condition is FRS = 800 rad·s^{-1} and WFR is 0.264 L·min^{-1} when the inlet air/water temperatures are both 45 °C [37]. The WFR of 0.264 L·min^{-1} is chosen for ALCSs in the IT room. Under this WFR condition, the water pressure drop of ALCS is 149.32 Pa, and the water outlet temperature is 74 °C, while the maximum temperature of CPU chips is 84.24 °C. Every rack has eleven ALCSs, and the typical IT room unit consists of twenty racks. The heat dissipation rate of the typical IT room unit is 117.4 kW. The rated cooling capacity of the air-cooled chiller is 510 kW. A single air-cooled chiller can be matched with four typical IT room units, and the total heat dissipation rate reaches 469.6 kW. The DC corresponding to a single air-cooled chiller is treated at the smallest DC typical unit for the analysis of DC cooling performance in this paper. It has 80 racks, 40 AHUs, one MPHE, and one air-cooled chiller.

2.4. The DC performance evaluation method

The whole DC performance is simulated by the above mathematical models coded in MATLAB SIMULINK. The one-year simulation and the ten-year simulation are conducted. For the one-year case (2023), the simulation duration is 8760 h, and the simulation time step is 0.1 h. For the ten-year case (2014–2023), the simulation duration is 87,648 and the simulation time step is 0.1 h.

As for the cooling performance of DC, the *COP* and *PUE* (power usage effectiveness) are adopted as the evaluation indexes. The studied DC typical unit consists of servers' load, cooling system load, and the additional components load.

COP of the DC typical unit indicates the effectiveness of the cooling system, which is calculated by:

$$COP = \frac{Q_{servers}}{P_{AHU\text{-}fans} + P_{server\text{-}fans} + P_{water\text{-}pump} + \left(Q_{cold\text{-}plate}/COP_{chiller}\right)} \quad (11)$$

where, $Q_{servers}$ is the total heat dissipation power of servers, W; $P_{AHU\text{-}fans}$ is the total fans power of AHU, W; $P_{server\text{-}fans}$ is the total power of fans in servers, W; $P_{water\text{-}pump}$ is the total power of pumps in the water-cooling system, W; $Q_{cold\text{-}plate}$ is the total heat dissipation rate of cold plates via water, W.

The *PUE* of the DC typical unit is calculated by **Eq. (12)**.

$$PUE = \frac{P_{servers} + P_{AHU\text{-}fans} + P_{server\text{-}fans} + P_{water\text{-}pump} + \left(Q_{chiller}/COP_{chiller}\right) + P_{additional}}{P_{servers}} \quad (12)$$

where, $P_{additional}$ is the power loss of power distribution and lighting, which is treated as 5 % of total server power, W; $P_{servers}$ is the total server components' electric power, W. In this paper, the electric power of the server is regarded as the same as the total heat dissipation power.

In **Eq. (11)** and **Eq. (12)**, from the aspect of the heat transfer process, the server components' electric/heating power and server fans' power are separated. The server fans are treated as part of the cooling system. Although such treatment causes lower *COP* and higher *PUE*, it is more reasonable to treat the fan's power as one part of the cooling system's power.

The server power is treated as constant in this paper, while the cooling system power is influenced by the environment temperature. The historical environment temperature of Xi'an is used as environment temperature data. The ten-year historical environment temperature (from 2014 to 2023) is provided by PVGIS [44], which is given in the Supplementary Material 2. The highest historical environment temperature is 38.7 °C, then the upper limit of 40 °C is treated as the highest environment temperature of the studied DC.

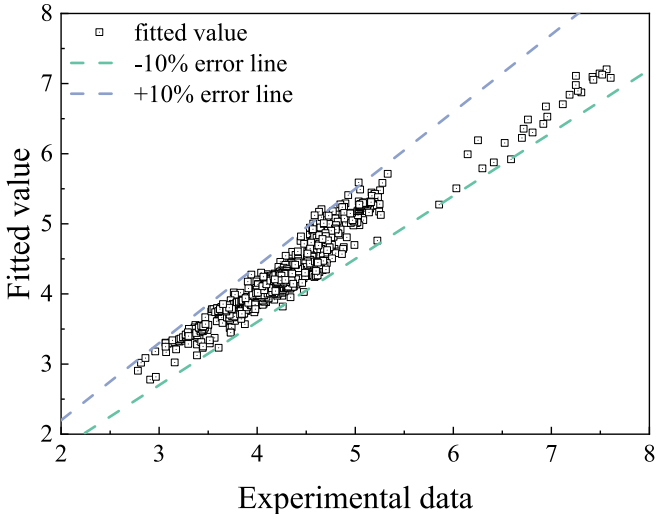

Fig. 10. The relative deviation of the chiller *COP* fitting result and experimental data.

3. Results and discussion

In this Section, the cooling performance of the typical IT room under different FRS working conditions is first introduced. And a modified FRS working condition is chosen for the typical IT room. Then, the AHU coupling performance is studied, and an optimized applicable AHU heat exchanger is chosen. Finally, the overall cooling and energy consumption performance of DC is analyzed and discussed.

3.1. The effects of FRS on room-level cooling performance

There are eleven ALCSs in one rack, and every ALCS has six small fans. In this paper, the FRS of the six fans in identical servers is the same, while the FRS of fans in different servers can be different values. The FRSs in different ALCSs are the key operation conditions of the ALCS air-cooling part, and the FRS configurations in the rack are crucial for the energy saving of DC. This subsection aims to obtain modified FRS working conditions with a good cooling effect and energy-saving effect for the ALCS in the studied IT room unit.

The cooling performance under the conditions that the FRS is constant for all fans in the rack is studied first in this subsection. The test FRS range is 500–1500 rad·s^{-1}, and the inlet air temperature is 45 °C for all cases. Fig. 11 shows the simulation results of the maximum temperature of HDDs, power units and memories, and total fan power under different FRS conditions. The fan power calculation method can be found in [37]. It is clear that, under the same FRS, the memories have the maximum temperature, followed by the power units, and the HDD has the lowest temperature. The maximum temperatures of all components decrease with the increase of FRS. Under the condition that all components are working under their limit temperature (60 °C for HDD, 95 °C for memory, and 105 °C for power units), the minimum FRS is 850 rad·s^{-1} as shown in Fig. 11, in which the maximum temperature of

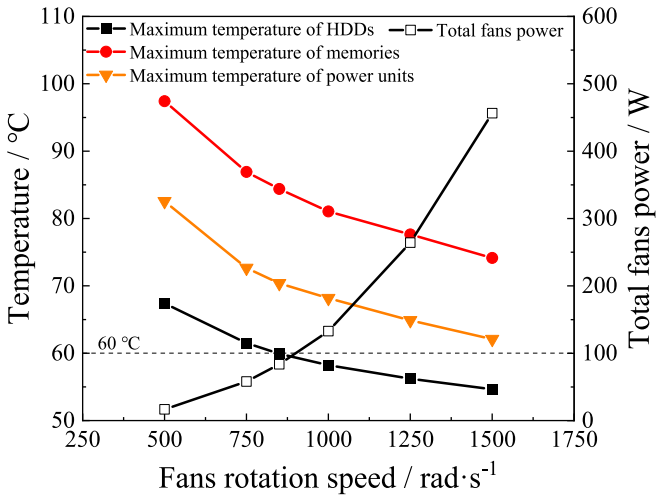

Fig. 11. The maximum temperature of HDDs, power units, and memories, and total fan power versus FRS when FRS is constant for all ALCSs.

HDDs, power units and memories are respectively 59.93 °C, 70.39 °C, and 84.39 °C. Only the maximum temperature of HDDs reaches the limit temperature, and the maximum temperatures of power units and memories are both much lower than their limit temperature. It means HDDs are the main barrier to reducing FRS since the limit temperature is only 15 °C higher than the inlet air temperature. In summary, when all fans have the same FRS, the minimum FRS is 850 rad·s^{-1} due to the temperature limit of HDDs, and the total fan power of eleven ALCSs in one rack is 83.68 W. By replacing the original air-cooled heat sink of CPU-packages with cold plate, the cooling requirement of air-cooling part is greatly reduced and the FRS can be reduced to a low value (850 rad·s^{-1}). As we can see in Fig. 11, the total fan power under the maximum FRS reaches 456.4 W, while the total fan power under the FRS of 850 rad·s^{-1} is only 83.68 W for eleven servers in the rack; the total fan power is reduced by 82 % while all components are working under safe temperatures.

The streamlines and temperature contours at the cross-section of the IT room and the 3D air streamlines distribution in the IT room are shown in Fig. D-1 in **Appendix. D**. The cross-section of the IT room passes through the HDD, memory, and power unit. As we can see from Fig. D-1 (a) to Fig. D-1(c), when FRS is as low as 500 rad·s^{-1}, the high-temperature region occurs at the memories' and power units' cross-sections. When FRS is improved to 1000 rad·s^{-1}, the improved air volume flow rate causes better cooling performance, and the high-temperature region almost disappears. As for the limit FRS of 850 rad·s^{-1} mentioned above, the high-temperature region is also small; the highest temperature occurs at the 9th server from the bottom to up. The streamline pattern is mainly influenced by the air inlet/outlet location of the IT room. As we can see in Fig. D-1, there is a large vortex and a small vortex in the cold aisle for all FRS cases. The small vortex is located at the entrance of the upper ALCSs in the rack, which blocks the inlet air of these servers (the highest three servers); the air needs to flow bypass the small vortex to enter the highest servers. For the other ALCSs, air can enter the servers more smoothly, as shown from Fig. D-1(d) to Fig. D-1 (f). The air in the cold aisle is forced by the fans and flows through the air zones in ALCSs, and finally enters the hot aisle. It is worth noting that some vortexes and reversed flows occur in the air zones between the ALCSs. This phenomenon is caused by the high-pressure region at the hot aisle around these servers. The low-velocity air exiting the server is reversed and flows into the air zone above the server, which forms the reversed flows and vortexes. In other Y cross-sections, the high-velocity air directly flows into the hot aisle. The air-cooling performance is mainly affected by the air flow in the ALCS. The reverse flows above the ALCS have little influence on the cooling of HDDs, memories, and power units in the server. Thus, further discussion on the reversed flows above the ALCSs is not provided here.

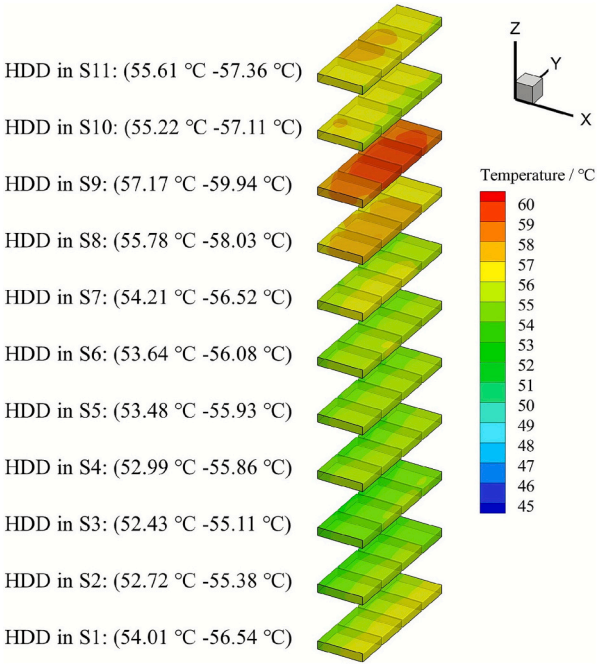

Fig. 12. The temperature distribution of HDDs when FRS is 850 rad·s^{-1}.

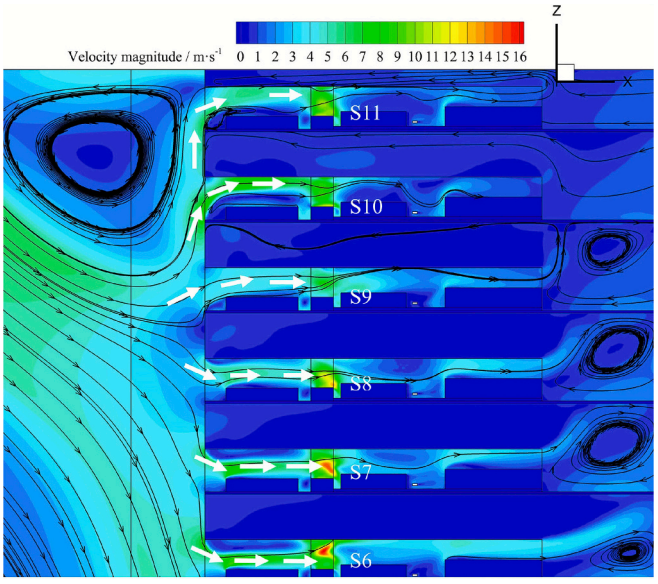

Fig. 13. The enlarged view of streamlines and temperature contour around S9 when FRS is 850 rad·s^{-1}.

When FRS is the same for all ALCSs, the lowest FRS is 850 rad·s^{-1} to ensure the safe operation of HDDs. Fig. 12 shows the temperature distribution of HDDs when FRS is 850 rad·s^{-1}, in which the server is named "S1" to "S11" from bottom to up in the rack. It is clear that the highest temperature occurs at the HDDs in "S9", which is 59.94 °C. And the highest HDD temperature of other servers is 58.03 ("S8"), which is 1.9 °C lower than "S9". Fig. 13 shows the enlarged view of the streamline and temperature contour around "S9". There is a small vortex at the front of "S10" and "S11", which blocks the air inlet of "S9", "S10", and "S11". The air needs to flow around the vortex before it flows into the server. This makes the inlet airflow direction of "S9", "S10" and "S11" upward, that is, the air will first impinge the up-wall of the server rather

than the HDD wall, which makes the air velocity near the HDD wall is small for “S9”, “S10”, and “S11” as shown in Fig. 13. The low near wall velocity causes poor heat dissipation performance of HDD in “S9”, “S10”, and “S11”, which is corresponding to the HDDs temperature distribution in Fig. 12. In Fig. 13, the inlet airflow direction is downward for “S8”, “S7”, and “S6”, while the near wall velocity is also higher for these servers. The air impingement on the HDD wall causes better cooling performance, and the maximum HDD temperatures of “S6”, “S7”, and “S8” are much less than “S9”.

In summary, affected by the small vortex in the front of “S10” and “S11”, the incoming air of “S9” has a small velocity and upward flow direction, which causes poor cooling performance of HDDs in “S9”. The maximum HDD temperature of “S9” reaches 60 °C, while the maximum HDD temperatures of the other ALCSs are 2 °C to 4.9 °C lower than 60 °C, as shown in Fig. 12.

In the above cases, all fans in the servers operate under the same FRS. In real DC, the FRS of different servers can be adjusted by controllers. FRS of different ALCSs is controlled by the fan controllers in the server or a lump controller in the IT room. Thus, the FRS in different ALCS can be set to different values. In this paper, modified FRS conditions for the studied rack are tested. For “S9” and the server with a higher HDD temperature in Fig. 12, the FRS is improved to enhance the HDD cooling performance. For the servers with lower HDD temperatures, like “S2”, “S3”, and “S4” in Fig. 12, the FRS is reduced to save fan power. It is expected to obtain a modified rack-level FRS condition with better cooling performance and lower total fan power compared with the constant FRS case of 850 rad·s^{-1}. The modified FRS conditions are based on uniform FRS conditions in Fig. 11 (FRS = 850 rad·s^{-1} for all fans), which is named “850-basic”. Four adjustment strategies are adopted, as shown in **Tables 2 to 5**. In the tables, “+”, “-”, and “o” are three FRS adjustment symbols, representing the FRS increase, decrease, and constancy based on FRS = 850 rad·s^{-1}. For each FRS adjustment strategy in the same table, the single symbol respectively represents the FRS adjustment step of 50 rad·s^{-1}, 100 rad·s^{-1}, 200 rad·s^{-1}, and 300 rad·s^{-1} for different cases, while the FRS has a limit range of 450 rad/s to 1450 rad/s. The detailed server FRS of the tested cases in **Tables 2 to 5** is calculated by the basic FRS (850 rad·s^{-1}) and their FRS adjust symbols. Here take the FRS adjustment strategy one in Table 2 as an example, the FRS adjust symbols of “S1” is “o”, it means the FRS of “S1” is not changed and keeps as 850 rad·s^{-1} for all three cases (“850-case-1”, “850-case-2”, and “850-case-3”) in Table 2; the FRS adjustment symbols of “S2” is “–”, it means the FRS of “S2” is decreased with a double of FRS adjustment steps. With the change of cases from “850-case-1” to “850-case-3”, the FRS of “S2” are respectively 750 rad·s^{-1} (850–50 × 2), 650 rad·s^{-1} (850–100 × 2), and 450 rad·s^{-1} (850–200 × 2) for “850-case-1”, “850-case-2”, and “850-case-3”. The detailed FRSs for all tested cases are obtained by combining the basic FRS (850 rad·s^{-1}) and every server’s FRS adjustment symbols. In this paper, 13 kinds of FRS adjustment cases based on “850-basic” are tested, which are given in **Tables 2 to 5**.

Fig. 14 gives the maximum HDD temperature and total fan power of all 13 FRS adjustment cases. For the cases in the same FRS adjustment strategies, as shown in Fig. 14(a), the maximum HDD temperature decreases first and then increases with the change of case name. It indicates that the moderate adjustment of FRS can effectively enhance the HDD cooling performance, but the FRS adjustment degree should not be excessive. All four FRS adjustment strategies can reduce HDD maximum temperature. From strategy one to strategy four, the maximum HDD temperature can be reduced to 58.75 °C (“850-case-2”), 57.67 °C (“850-case-5”), 58.04 °C (“850-case-8”), and 57.22 °C (“850-case-12”). Among the 13 cases, “850-case-12” achieves the lowest maximum HDD temperature of 57.22 °C, which is 2.71 °C lower than the basic case (“850-basic”). However, the total fan power of “850-case-12” is 89.19 W, which is 5.51 W higher than “850-basic”. For the modified case, the total fan power is required to be less than the basic case, while the maximum HDD temperature should be as low as possible. Under this condition, the optimized FRS condition is “850-case-5” among the 13 cases; it has a total fan power of 81.36 W (2.32 W less than “850-basic”) while the maximum HDD temperature is 57.67 °C (2.27 °C less than “850-basic”). The maximum temperatures of memories and power units of “850-case-5” are respectively 87.5 °C and 75.2 °C, which are both less than their limit temperature (95 °C and 105 °C).

In summary, for the proposed 13 FRS adjustment cases based on “850-basic”, the optimized FRS modified condition is “850-case-5”, which reduces the maximum HDD temperature by 2.27 °C and the total fan power by 2.32 W compared with “850-basic”.

3.2. The cooling performance of AHU in DC

This subsection will give and discuss the free-cooling performance after combining AHU based on the optimized IT room cases “850-case-5”. An optimized AHU heat exchanger type with the highest cooling efficiency is obtained among all twelve types of AHU configurations. The key CFD simulation results of “850-case-5” are summarized here: the inlet air temperature of the IT room is 45 °C, the outlet temperature of the IT room is 48.15 °C, and the air volume flow rate for one rack is 1.095 m^3·s^{-1}. The smallest DC typical unit studied in this paper has 80 racks and 40 AHUs. Two adjacent racks share one AHU heat exchanger. One AHU must cool the hot air with a volume flow rate of 2.19 m^3·s^{-1} from 48.15 °C to not higher than 45 °C. The heat dissipation rate is about 8292.5 W for one AHU. Based on the $q_{v\text{-}c}$ (cold-side air flow rate) calculation method and $P_{AHU\text{-}fans}$ (AHU fans power consumption) calculation method introduced in **subsection 2.2**, **Fig. 15** gives the $q_{v\text{-}c}$ and $P_{AHU\text{-}fans}$ versus environment temperature plots for all twelve AHU heat exchanger designs within the environment temperature range of 15 °C–40 °C.

As shown in **Fig. 15**, all AHU heat exchangers can effectively cool the IT room outlet air when the environment temperature is 15 °C, the cold side of AHUs is working under the lowest $q_{v\text{-}c}$. With the increase of environment temperature, $q_{c\text{-}v,}$ and $P_{AHU\text{-}fans}$ start to increase when environment temperature is higher than a specific temperature for all AHUs. When the environment temperature is as high as 40 °C, some heat exchangers with poor heat dissipation ability (“H12-basic”, “H12R10h2”, “H12R10h3”, and “H10-basic”) have been unable to meet the cooling requirement of the IT room. As shown in **Fig. 15(a)**, **Fig. 15 (b)**, **Fig. 15(c)**, and **Fig. 15(e)**, the $q_{v\text{-}c}$ of AHU has reached its maximum value when the environment temperature is less than 40 °C. When the environment temperature is 40 °C, the effect of free-cooling is greatly reduced, and the $P_{AHU\text{-}fans}$ are high for most AHUs. Among the twelve

Table 2
Servers FRS of adjustment strategy one.

	FRS of servers										
Server name	S1	S2	S3	S4	S5	S6	S7	S8	S9	S10	S11
FRS adjustment symbol	o	–	–	–	–	–	o	+	++	o	+
850-case-1	850	750	750	750	750	800	850	900	950	850	900
850-case-2	850	650	650	650	650	750	850	950	1050	850	950
850-case-3	850	450	450	450	450	650	850	1050	1250	850	1050

Table 3
Servers FRS of adjustment strategy two.

	FRS of servers										
Server name	S1	S2	S3	S4	S5	S6	S7	S8	S9	S10	S11
FRS adjustment symbol	o	–	–	–	–	–	o	++	+++	++	++
850-case-4	850	750	750	750	750	750	850	950	1000	950	950
850-case-5	850	650	650	650	650	650	850	1050	1150	1050	1050
850-case-6	850	450	450	450	450	450	850	1350	1450	1350	1350

Table 4
Servers FRS of adjustment strategy three.

	FRS of servers										
Server name	S1	S2	S3	S4	S5	S6	S7	S8	S9	S10	S11
FRS adjustment symbol	o	–	–	–	–	–	o	+	+++	+	+
850-case-7	850	750	750	750	750	750	850	900	1000	900	900
850-case-8	850	650	650	650	650	650	850	950	1150	950	950
850-case-9	850	450	450	450	450	450	850	1050	1450	1050	1050

Table 5
Servers FRS of adjustment strategy four.

	FRS of servers										
Server name	S1	S2	S3	S4	S5	S6	S7	S8	S9	S10	S11
FRS adjustment symbol	o	–	–	–	–	–	o	+	+++	+	+
850-case-10	850	800	800	800	800	800	850	900	1000	900	900
850-case-11	850	750	750	750	750	750	850	950	1150	950	950
850-case-12	850	650	650	650	650	650	850	1050	1450	1050	1050
850-case-13	850	550	550	550	550	550	850	1150	1500	1150	1150

AHU designs, the "H7.5R10h3" performs best when the environment temperature is 40 °C, which has a low $P_{\text{AHU-fans}}$ of 2.1 kW. Although some other AHU designs can meet the heat dissipation requirement of IT room air circulation, their $P_{\text{AHU-fans}}$ are all higher than "H7.5R10h3". The highest even reaches 10.8 kW ("H10R10h2" in **Fig. 15(f)**). "H7.5R10h3" is suitable for the high-temperature environment rather than the low-temperature environment, since it has a high $P_{\text{AHU-fans}}$ of 1.1 kW when the environment temperature is small as shown in **Fig. 15 (k)**.

To intuitively compare the cooling performance of different AHU designs, Fig. 16 gives the COP_{AHU} versus environment temperature for all AHU designs. When the environment temperature is low, COP_{AHU} does not change with the environment temperature. This is because the cold side of AHU keeps working at the minimum $q_{\text{v-c}}$, and the heat dissipation power and $P_{\text{AHU-fans}}$ are constant. With the increase of environment temperature, $P_{\text{AHU-fans}}$ increase with the increase of $q_{\text{v-c}}$ until the maximum $q_{\text{v-c}}$ is reached. In this process, COP_{AHU} gradually decreases for all AHUs. For the same "H" series AHUs, the AHU design with the highest COP_{AHU} changes with the environment temperature increase. Take "H10" series for example, when the environment temperature range are respectively 15 °C - 33 °C, 34 °C - 36 °C, 37 °C - 38 °C, and 39 °C - 40 °C, the AHU designs with highest COP_{AHU} are respectively H10-basic, H10R10h2, H10R10h3, and H10R10h4 as shown in Fig. 16 (b). It can be seen that the AHU with higher spherical dimple depth has higher COP_{AHU} under high environment temperature, while the AHU with the basic flat plate has higher COP_{AHU} under low environment temperature. When the environment temperature is 15 °C, the highest COP_{AHU} reaches 28 for "H12-basic". The high COP_{AHU} is caused by the high heat transfer temperature difference and low flow resistance of cold air. The inlet hot air temperature of AHU is 45 °C, which is 30 °C higher than the cold air inlet temperature (15 °C). Thus, "H12-basic" can work at the lowest cold air volume flow rate of 0.65 $m^3 \cdot s^{-1}$. And the cold side air pressure drop is only 10.16 Pa under the lowest air volume flow rate (0.65 $m^3 \cdot s^{-1}$). The energy consumptions of the hot-side fan and cold-side fan are respectively 281.20 W and 15.12 W, while the AHU provides 8292.5 W of cooling power. However, COP_{AHU} decreases rapidly with the increase of environment temperature. When the environment temperature is higher than 35.3 °C, "H12-basic" can't meet the cooling requirement of the IT room, in which condition AHU design with higher heat dissipation ability is required. As shown in Fig. 16(a), for the "H12" series, only "H12R10h4" achieves effective cooling of air circulation when the environment temperature is 40 °C, but the COP_{AHU} is only 1.28. To further improve COP_{AHU} under the environment temperature of 40 °C, the AHU with a smaller channel height can be adopted. As shown in Fig. 16(b) and Fig. 16(c), when the environment temperature is 40 °C, the "H10" series AHU achieves the highest COP_{AHU} of 2.31 ("H10R10h4"), and the "H7.5" series AHU achieves the highest COP_{AHU} of 3.94 ("H7.5R10h3").

As can be seen from the above analysis, the AHU designs with small flow resistance and poor heat dissipation ability (like "H12-basic") achieve higher COP_{AHU} under low environment temperature, but they can't provide enough cooling capacity under high environment temperature, their COP_{AHU} is quickly reduced with the increase of environment temperature. The AHU designs with strong heat transfer ability and large flow resistance can provide enough cooling capacity under high environment temperature with relatively high COP_{AHU}, but they have higher COP_{AHU} when the environment temperature is low. For example, "H7.5R10h3" has a COP_{AHU} of 5.16 when the environment

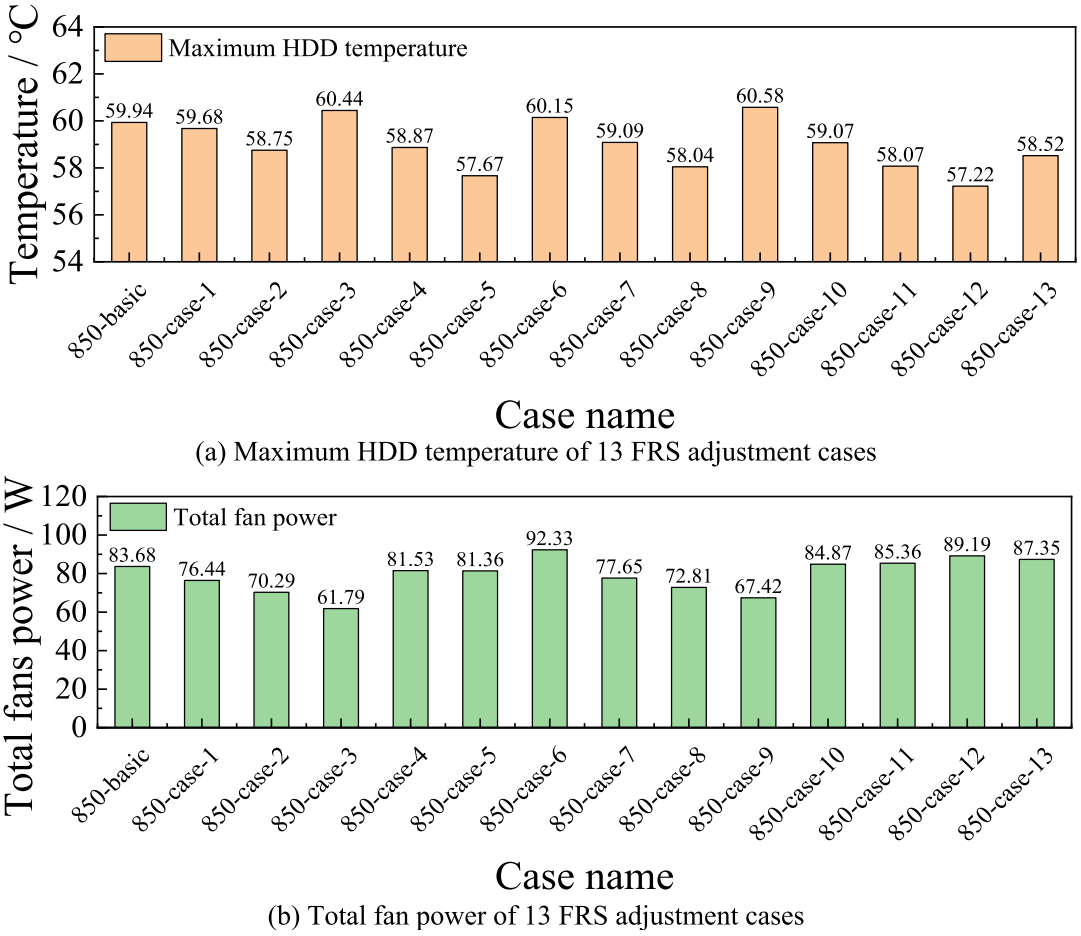

Fig. 14. Maximum HDD temperature and total fan power of 13 FRS adjustment cases. (a) Maximum HDD temperature of 13 FRS adjustment cases. (b) Total fan power of 13 FRS adjustment cases.

temperature is 15 °C, which is much lower than "H12-basic". It can be seen that, for DC, the selection of a suitable AHU design should comprehensively consider the environment temperature range of the DC location city. When the environment temperature is generally low and the maximum environment temperature is not high, the AHU design with weak heat dissipation ability and low flow resistance is more suitable. When the environment temperature is generally high and the maximum environment temperature is also high, the AHU design with strong heat dissipation ability should be chosen to ensure the cooling requirement of the IT room.

In this paper, the studied DC is located at Xi'an, and the historical environment temperature data from 2014 to 2023 are adopted for AHU performance evaluation. Fig. 17 shows the ten-year averaged COP_{AHU} for all AHU designs, the "H12-basic", "H12R10h2", and "H10-basic" are the not applicable AHU design for the studied DC, since they can't provide the required cooling capacity when environment temperature is as high as 38.7 °C (the highest historical environment temperature), and there is a risk of failure in the thermal management of the IT room. As for the other AHU designs, the highest averaged COP_{AHU} is 17.54 for "H7.5-basic", which is more suitable for the studied DC compared with other AHU designs. Xi'an has generally low environment temperature, with high environment temperature occurring in summer. The AHU designs with small flow resistance and poor heat dissipation ability are more suitable for DC in Xi'an. As shown in Fig. 17, the optimized AHU design for the studied DC in Xi'an is "H7.5-basic"; it can cool the IT room circulation air when the environment temperature is as high as 38.7 °C and achieves a high ten-year averaged COP_{AHU} of 17.54.

3.3. The overall cooling and energy consumption performance of DC in Xi'an

The modified IT room working condition ("850-case-5") and the optimized AHU design ("H7.5-basic") are obtained in the above subsections. This subsection will further provide the performance of the water-cooling system of the studied DC, and then the overall cooling and energy consumption performance of the DC is given and discussed.

Table 6 summarizes the main components' information of the studied typical DC unit, including the ALCS, rack, MPHE, air-cooled chiller, and AHU. The ALCS in our previous work [37] is adopted in the DC, which has a 2 U size, and eleven ALCSs are integrated in one rack. The typical DC unit has 80 racks and 880 ALCSs. For one rack in the typical DC unit, the total fan power is 81.36 W. The total heat dissipation rate of servers is 801.3 kW, in which the heat dissipation rates of AHUs and air-cooled chiller are 331.7 kW and 469.6 kW. The chosen AHU heat exchanger design is "H7.5-basic"; the fan power of the AHU is influenced by the environment temperature. The indoor part of the water-cooling system is the water pipe system, and a typical water pipe system consists of ten parallel racks. For the typical water pipe system, the total pressure drop is 5591.93 Pa and the water volume flow rate is 4.84×10^{-4} $m^3 \cdot s^{-1}$. A typical DC unit has 8 typical water pipe systems, which are arranged in parallel. The IT room outlet water temperature is 74 °C, and the outlet water is cooled to 45 °C in MPHE by the chiller supply water with a constant temperature of 10 °C. After the heat transfer in MPHE, the cold-side outlet water of the MPHE is set at 15 °C, which is transported back to the air-cooled chiller. The MPHE should be designed to meet the above heat transfer requirement. A qualified MPHE design is

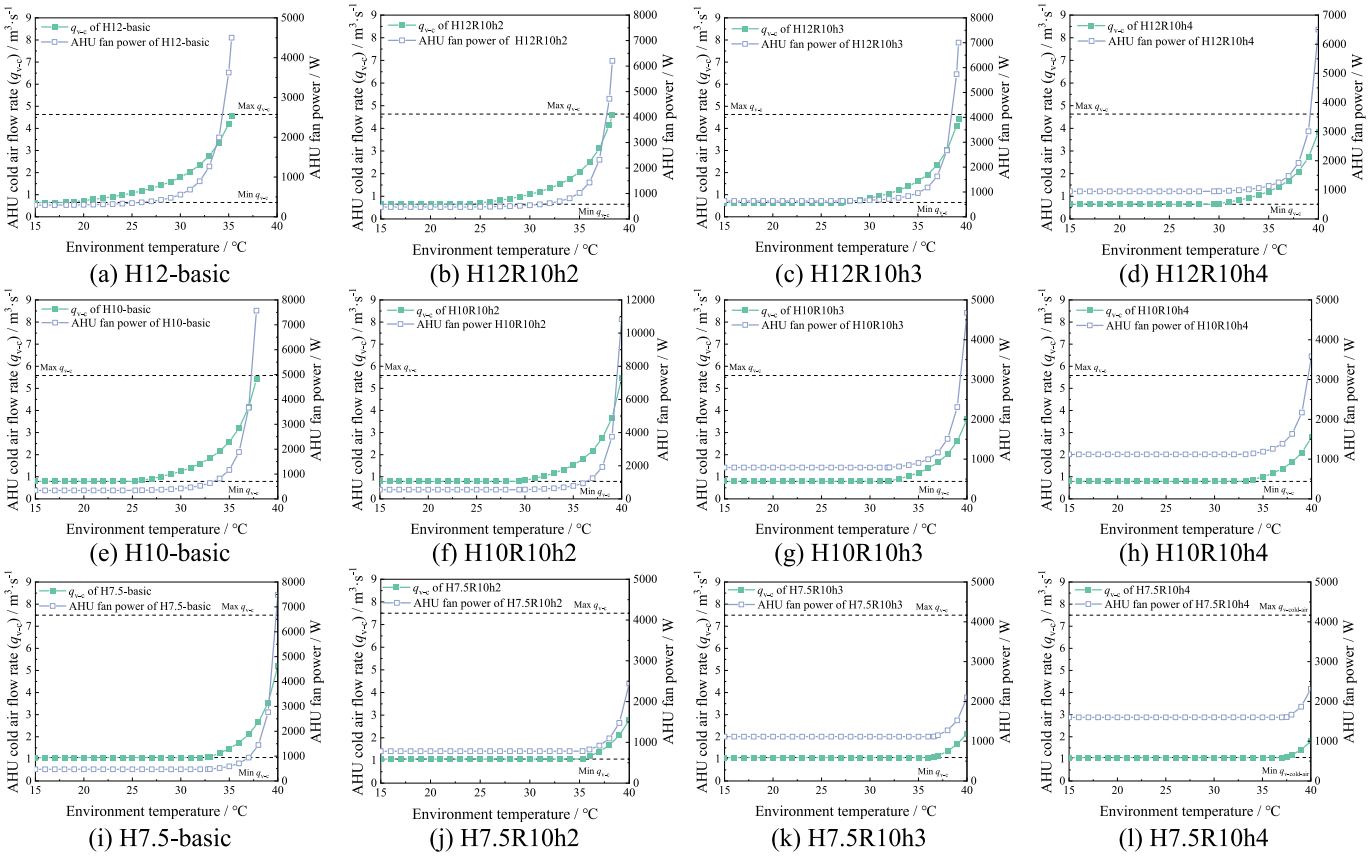

Fig. 15. $q_{v\text{-}c}$ and $P_{AHU\text{-}fans}$ versus environment temperature plots for all twelve AHU heat exchanger designs (based on IT room FRS condition of "850-case-5").

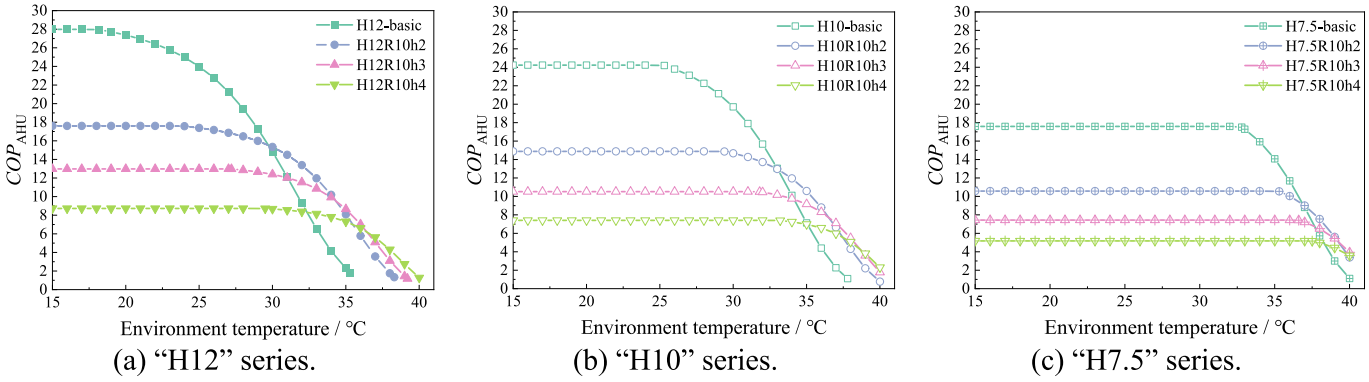

Fig. 16. COP_{AHU} versus environment temperature for all twelve AHU designs. (a) "H12" series. (b) "H10" series. (c) "H7.5" series.

obtained by HTRI Xchanger Suite, and the detailed design result is given in the **Appendix. C**. Table 7 gives the key design results of the MPHE adopted in the studied DC. The water flow rate (WFR) of the chiller side is 22.395 kg·s^{-1}. The pressure drop of the IT room side and chiller side are respectively 1.487 kPa and 39.099 kPa. The heat exchange rate of MPHE is 470 kW, and the overdesign is 36.54 %. The *COP* of the air-cooled chiller is calculated by **Eq.**(10), and the chiller electric power is obtained by the chiller *COP* and the chiller's working cooling capacity.

Based on the IT room CFD simulation results, AHU model, water-pipe system pressure drop calculation results, MPHE design results, and the *COP* fitting formula of the air-cooled chiller. The overall cooling and energy consumption of the studied typical DC unit under different environment temperatures can be calculated. Fig. 18 gives the environment temperature, *COP*, and *PUE* versus real time for a typical hot/cold day of the studied DC in Xi'an. As shown in Fig. 18(a), on a typical hot day, the highest and lowest environment temperature are respectively 38.7 °C and 26.5 °C. The performance of the cooling system varies with the environment temperature fluctuations. When the environment temperature increases from 26.5 °C to 38.7 °C, the *PUE* increases from 1.21 to 1.35, and the *COP* of DC decreases from 6.10 to 3.37. Under the highest environment temperature of 38.7 °C, a total cooling power of 237.8 kW is required for the typical DC unit with 801.3 kW of server load. Environment temperature has a greater influence on COP_{AHU} than $COP_{chiller}$ in the typical hot day, as shown in Fig. 18(a). When the environment temperature is lower than 32.6 °C, AHU maintains a high COP_{AHU} of 17.59. When the environment temperature is increased to 38.7 °C, COP_{AHU} has decreased to 3.75. The reason why COP_{AHU} decreases significantly as the environment temperature rises is that the environment temperature is very close to the hot-side air outlet temperature (45 °C) of the AHU. The heat transfer temperature difference of

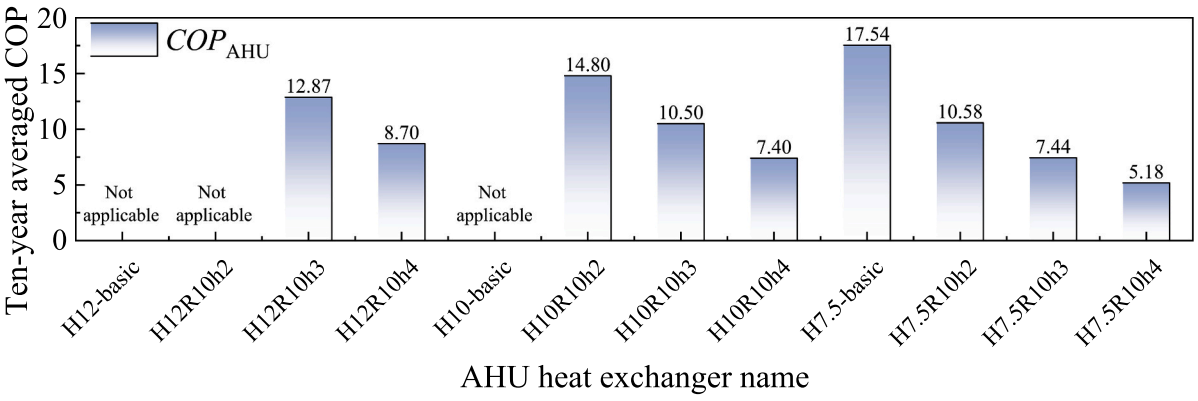

Fig. 17. Ten-year averaged COP_{AHU} for all twelve AHU designs.

Table 6
The information of the main components in the typical DC unit (850-case-5).

Component information	Value	Component information	Value
Number of servers	880	Number of AHU	40
Servers power	801.3 kW	AHU heat exchanger design	H7.5-basic
Number of racks	80	AHU working cooling capacity	331.7 kW
Chiller number	1	MPHE number	1
Chiller rated/working cooling capacity	510 kW/ 469.6 kW	MPHE working heat transfer rate	469.6 kW

Table 7
The key design results of MPHE adopted in the DC.

Parameter	Value	Parameter	Value
IT room side WFR	3.865 $kg{\cdot}s^{-1}$	Chiller side WFR	22.395 $kg{\cdot}s^{-1}$
IT room side water inlet temperature	74.05 °C	Chiller side water inlet temperature	10.00 °C
IT room side water outlet temperature	44.98 °C	Chiller side water outlet temperature	15.01 °C
IT room side water pressure drop	1.487 kPa	Chiller side water pressure drop	39.099 kPa
Heat transfer rate	470 kW	Overdesign	36.54 %

AHU decreases rapidly when the environment temperature is increased from 32.6 °C to 38.7 °C. However, it is worth noting that COP_{AHU} is always higher than $COP_{chiller}$ on the typical hot day, which indicates that the cooling performance of AHU is always better than the traditional air-cooled chiller, especially when the environment temperature is below 32.6. On the typical hot day, during the time when the environment temperature is higher than 32.6 °C, AHU keeps high COP_{AHU} during the afternoon and night. $COP_{chiller}$ is also increased for these hours of the day. The day-averaged *PUE* of DC is only 1.25 for the typical hot day. The DC has better cooling performance on the typical cold day, as shown in Fig. 18(b), the day-averaged *PUE* of DC is only 1.15, and the day-averaged *COP* of DC, COP_{AHU}, and $COP_{chiller}$ are respectively 10.12, 17.59, and 8.95. The day-averaged cooling power consumption is only 79.2 kW for the typical cold day. As we can tell from the typical day performance of the DC, the integration of the free-cooling part (AHU)

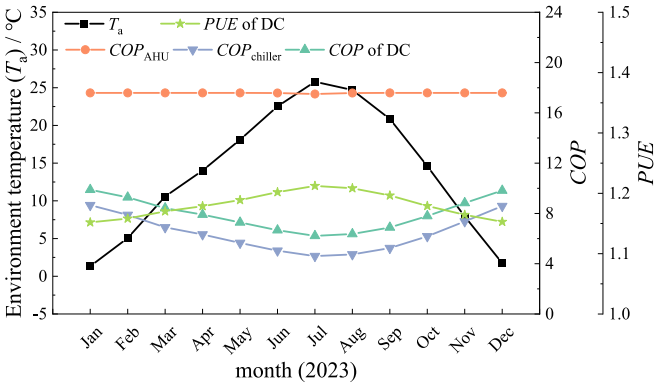

Fig. 19. The month-averaged environment temperature, *PUE*, and *COP* at different months for the proposed DC in 2023.

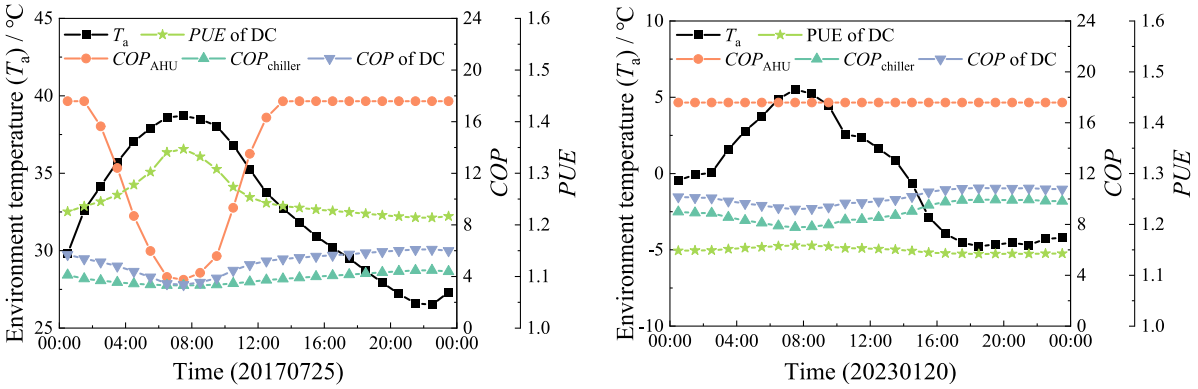

Fig. 18. Environment temperature, *COP*, and *PUE* versus real time for a typical hot/cold day of the studied DC in Xi'an. (a) The typical hot day (2017/07/25). (b) The typical cold day (2023/01/20).

helps to reduce the energy consumption of the cooling system. For the studied DC in Xi'an, COP_{AHU} is always higher than $COP_{chiller}$, especially when the environment temperature is lower than 32.6 °C. The proposed DC can achieve a low *PUE* of 1.15 for the typical cold day. For the typical hot day, the day-averaged *PUE* of DC is 1.25, which is still much lower than most traditional air-cooled DC [17,38,45].

Fig. 19 shows the month-averaged environment temperature, *PUE*, and *COP* at different months for the proposed DC in 2023. The highest month-averaged environment temperature is 25.8, which occurred in July. And the lowest month-averaged environment temperature is 1.33, which occurred in January. The month-averaged *PUE* of DC ranges from 1.15 to 1.21 in the year. The highest *PUE* occurs in July. The month-averaged COP_{AHU} is relatively stable, remaining at around 17.5. The month-averaged $COP_{chiller}$ has a larger range of 4.61–8.66, and the lowest $COP_{chiller}$ also occurs in July. With the energy-saving effect of AHU cooling, the month-averaged *COP* of the DC ranges from 6.22 to 9.88. From the above results on the daily performance and monthly performance, it can be seen that the environment temperature fluctuation has a great influence on the efficiency of both the AHU and chiller, which affects the *PUE* and *COP* of DC. However, it is worth indicating that the environment temperature has little influence on the cooling of server components in the rack. This is due to that the working condition of the IT room is constant. The coolant inlet temperature and flow rate are constant and stable, and the maximum temperatures of all components are lower than the limit temperatures based on the CFD simulation results. From the point of view of heat transfer, the components are reliable, although the environment fluctuates with time.

The ten-year averaged energy consumption of the studied DC based on environment temperature from 2014 to 2023 is given in Fig. 20. As we can see, the free-cooling and liquid-cooling combined DC proposed in this paper exhibits effective cooling performance. The ten-year average *PUE* is 1.18, while the ten-year average *COP* is 7.64. The servers consume the largest proportion of energy consumption in DC, reaching 84.7 %, followed by the chiller, reaching 8.3 %. The additional equipment, including power distribution units and lighting, consumes 4.2 % of total DC energy. The AHU only consumes 2 % of the total DC energy. The fans in the servers and pumps respectively consume 0.7 % and 0.1 % of total DC energy. The total energy consumption proportion of the cooling system in the studied DC is 11.1 %, in which the free-cooling part is 2.7 % (AHU and fans in servers) and the water-cooling part is 8.4 % (chiller and water pumps). The electric power of the free-cooling part is 25.45 kW, and the cooling capacity of the free-cooling part is 331.7 kW. The electric power of the water-cooling part is 79.39 kW, while the cooling capacity of the water-cooled part is 469.6 kW. It can be seen that the *COP* of the free-cooling part and water-cooling part are respectively 13.03 and 5.92. The *COP* of the free-cooling part has reached 2.2 times the *COP* of the water-cooling part, which indicates that the application of AHU can effectively improve the cooling efficiency of DC.

3.4. The cooling performance of DC in two additional typical cities

The above results give the energy-saving performance of the proposed DC cooling scheme in Xi'an. Xi'an has a ten-year average environment temperature of 14.06 °C. To indicate the generalizable of the proposed liquid-cooling and free-cooling combined cooling scheme in different climate conditions, two typical cities are studied in this subsection. One is Harbin with a low ten-year average environment temperature of 5.11 °C, and another is Haikou with a high ten-year average environment temperature of 25.00 °C. The environment temperature of Harbin and Haikou is given in Supplementary Material 3. For comparison, the studied typical DC units in Harbin and Haikou are the same as the studied DC units in Xi'an; the information of the typical DC units is given in Table 6. Since the maximum environment temperatures of Harbin and Haikou are respectively 36.64 °C and 36.62 °C, which are both lower than the maximum temperature of Xi'an, the AHU type of "H7.5-basic" is applicable for DC in Harbin and Haikou. It is worth emphasizing that for the DC in extremely hot regions, the AHU type must be first estimated to find the most suitable type with enough cooling ability and the highest COP_{AHU}.

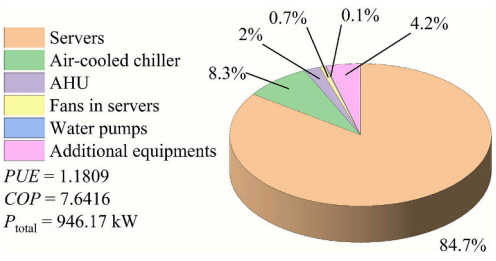

Fig. 20. The ten-year average energy consumption of the studied DC (from 2014 to 2023 in Xi'an).

The ten-year averaged energy consumption performance of the studied DC in Xi'an, Harbin, and Haikou is all given to show the energy-saving performance of the proposed DC cooling scheme. The DCs in the three cities have the same equipment arrangement. The only difference is the climate conditions. The ten-year DC operation simulations are conducted for the three cities, and the average components power is calculated based on the simulation results. Further, the averaged *COP* and *PUE* of the DCs in three cities are calculated by **Eq. (11)** and **Eq. (12)** based on the averaged data. The ten-year average energy consumption of DC in Xi'an is given in Fig. 20. For the studied DCs in Harbin and Haikou, Fig. 21 shows the ten-year average energy consumption results. For the typical DC unit in Harbin, the low environment temperature helps to save the cooling energy. The averaged total power is 932.96 kW, which is 13.21 kW lower than the P_{total} of the typical DC unit in Xi'an. For the typical DC unit in Harbin, the energy-saving effect of the cooling system mainly comes from the electrical power reduction of the air-cooled chiller. As shown in Fig. 21(a), the air-cooling chiller only consumes 7 % of P_{total}. For the typical DC unit in Haikou, the high environment temperature requires high cooling energy. The averaged total power is 969.10 kW, which is 22.93 kW higher than P_{total} of the typical DC unit in Xi'an. The air-cooling chiller consumes 10.4 % of P_{total}. For all the typical DC units in Harbin, Xi'an, and Haikou, the power consumption of AHU has no significant change. It indicates that the AHU has a good cooling performance for all studied cities, although the highest average temperature reaches 25.00 °C.

Harbin, Xi'an, and Haikou represent China's cold, temperate, and tropical regions, respectively. This paper studies the ten-year average performance of the proposed cooling architecture in the three cities. For the same typical DC units in Harbin, Xi'an, and Haikou, the ten-year averaged *PUE* are respectively 1.16, 1.18, and 1.21; and the ten-year averaged COP are respectively 8.74, 7.64, and 6.27. The proposed liquid-cooling and free-cooling combined DC cooling system can effectively save the cooling energy even in tropical regions like Haikou.

3.5. Discussion on the key findings and future work

This paper studied the cooling performance of a novel cooling scheme combining liquid-cooling and free-cooling. The key findings can be divided into three parts. First, the effects of FRS on room-level air-cooling performance are investigated by the CFD method, and a modified FRS condition in the rack is obtained. The high inlet air temperature causes the limited cooling capacity of the low-components, especially for the HDDs. The FRS adjustment test results indicate that the air-cooling part of the server in high-temperature DC can be enhanced by adjusting the FRS of the server with poor cooling performance, which has not been investigated in the present studies. Second, the application of AHU achieves effective free-cooling performance. The free-cooling is integrated for the low-cost cooling of air-circulation. Unlike most present high-temperature DC cooling schemes, the CRAC is replaced by the

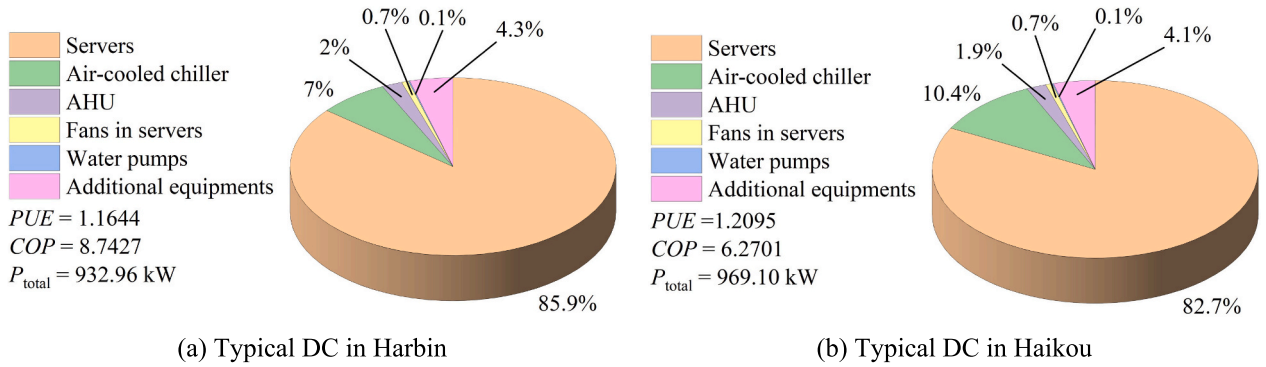

Fig. 21. The ten-year average energy consumption of the studied DC in Harbin and Haikou (from 2014 to 2023). (a) Typical DC in Harbin. (b) Typical DC in Haikou.

AHU. By adopting the high-performance AHU heat exchanger design, 100 % free-cooling for air-circulation in the IT room is achieved for all three cold, temperate, and tropical regions. Finally, this paper shows the complete DC cooling system design methods, including the CFD simulation of the IT room, ALCS, and AHU, and the system-level simulation of the whole DC cooling system. Because of natural cooling is inherently related to the local meteorological conditions, this paper has selected a data center in Xi'an for the case study. However, the methods and techniques of analysis are universal. The low *PUE* is achieved for the same typical DC units in Harbin, Xi'an, and Haikou. The proposed cooling scheme is generalizable for most climate conditions. The DC cooling system design methods adopted in this paper have more engineering application value than the existing work.

Although the cooling scheme performs effectively, the study in this paper is still limited by some simulation assumptions and boundary conditions:

1) The air and water are all adopts constant physical properties, also the effects of gravity and irradiance are ignored. These simplifications cause certain simulation errors.
2) The uniform heat sources of the components are not completely consistent with the actual components' working conditions.
3) The data transfer between the IT room and AHU is simplified, and the pipe system calculation method is simplified.

Considering the above limitations, the following future studies are recommended:

1) The simulation methods can be further developed by eliminating some assumptions like the physical properties, gravity, and irradiance.
2) The mechanism of uneven heat generation in chips should be further investigated, and the corresponding models for the CFD simulations at the whole chip scale are needed.
3) The lab-scale experiment is necessary to validate the practical performance in the real-world DC of the novel cooling scheme proposed in this paper. The data transfer between the IT room and AHU can be corrected by the experiment data. Also, the pipe system calculation methods can be corrected using the experimental data.
4) The waste heat recovery system is recommended to be integrated into the water-cooling system since the cold plate outlet water temperature reaches 74 °C, which is promising for waste heat recovery technologies, such as absorption cooling and district heating.

4. Conclusions

In this paper, a liquid-cooling and free-cooling combined DC in Xi'an is proposed and studied. The microchannel cold plate and AHU are applied for the energy-saving of the first cooling system and the second cooling system. First, a modified FRS condition ("850-case-5") of the servers in the rack is obtained. Then, an optimized AHU design is chosen based on the historical temperature data in Xi'an under the IT room condition of "850-case-5". Finally, the cooling and energy consumption performances of DC are given and discussed. The main conclusions are as follows:

1. The effects of FRS on the cooling of servers in the IT room are studied, and a modified FRS working condition is obtained. When the FRS is the same for all servers in the rack, the minimum FRS is 850 rad·s^{-1} to ensure all components are working under the limit temperatures. When FRS is 850 rad·s^{-1}, the maximum temperatures of HDDs, memories, and power units are respectively 59.93 °C, 84.39 °C, and 70.39 °C; and the total fan power of the rack is 83.68 W. HDDs are the main barrier to further reducing FRS, and HDDs in "S9" reach 60 °C. A modified FRS condition "850-case-5" is obtained by adjusting the FRS of different servers, which further reduces the maximum HDD temperature and fan power to 57.67 °C and 81.36 W compared with "850-basic".
2. The free-cooling performance of different AHU designs is investigated, and an optimized AHU design for the DC in Xi'an is chosen. It is found that all AHU designs can achieve the cooling requirement of IT room air circulation under the environment temperature of 15 °C, and the highest COP_{AHU} reaches 28 ("H12-basic"). When the environment temperature is as high as 40 °C, some AHU designs can't achieve the required heat dissipation rate, and the highest COP_{AHU} is 3.94 for "H7.5R10h3". For the studied DC in Xi'an, all AHU designs are tested under the ten-year historical environment temperature data, the best AHU design among the twelve AHU designs is "H7.5-basic", which can not only meet the cooling requirement of the IT room when the highest environment temperature is 38.7 °C but also has a high ten-year averaged COP_{AHU} of 17.54.
3. Based on the FRS condition of "850-case-5", the AHU type of "H7.5-basic", the calculated pressure drop of the water pipes system, the MPHE design results, and air-cooled chiller model, the cooling and energy consumption of a typical DC unit is obtained for typical hot/cold days, the month-averaged year and the ten-year average level. For the typical hot day, when the environment temperature is as high as 38.7 °C, the *PUE* of DC reaches 1.35, but the average *PUE* of the hot day is reduced to 1.25. For the typical cold day, the average *PUE* of DC is only 1.15. Whether it is a hot day or a cold day, the *PUE* of the proposed DC is much better than that of traditional air-cooled DC. In 2023, the month-averaged *PUE* of the studied DC ranges from 1.15 to 1.21. For the ten-year average level (from 2014 to 2023), the DC achieves a low *PUE* of 1.18 and a high *COP* of 7.64, in which the power consumption percentage of the free-cooling part (331.7 kW of cooling capacity) and water-cooling part (469.6 kW of cooling capacity) are respectively 2.7 % and 8.4 %.
4. For the same typical DC units in Harbin, Xi'an, and Haikou, respectively representing the cold, temperate, and tropical regions in China, the ten-year averaged *PUE* are respectively 1.16, 1.18, and

1.21, and the ten-year averaged *COP* are respectively 8.74, 7.64, and 6.27. It demonstrates that the proposed liquid-cooling and free-cooling combined DC cooling system can effectively save the cooling energy even in tropical regions. And the research methods employed in this paper are of general significance and can be used as a reference for DC in other regions with different climate conditions to reduce energy consumption.

CRediT authorship contribution statement

Zi-Xing Wang: Writing – original draft, Visualization, Validation, Software, Methodology, Investigation, Formal analysis, Data curation, Conceptualization. **Ke Xue:** Validation, Investigation. **Jun-Yu Chen:** Investigation. **Nan Li:** Investigation. **Wen-Quan Tao:** Writing – review & editing, Supervision, Resources, Funding acquisition.

Declaration of competing interest

The authors declare that they have no known competing financial interests or personal relationships that could have appeared to influence the work reported in this paper.

Acknowledgment

This work was supported by the Key Projects of National Natural Science Foundation of China [51836005, 51721004] and the Fund of Xi'an Science and Technology Bureau [2019218714SYS002CG024].

Appendix A

The AHU heat exchangers enhanced with spherical dimples and elliptic cylindrical dimples are studied by CFD simulation in our previous work [27,29]. Table A-1 shows the area-averaged convective heat transfer coefficient and pressure drop versus AHU working air flow rate (cold air or hot air) fitting formulas for all twelve AHU heat exchangers based on the CFD simulation results. The convection heat transfer coefficient and pressure drop are used for the calculation of AHU heat transfer rate and pressure drop (fans power loss). The calculation method can be found in [29]. The working flow rate range is based on the studied Reynolds number range for the AHUs.

Table A-1
Heat transfer coefficient and pressure drop fitting formulas of AHU heat exchangers.

AHU name	Area-averaged convection heat transfer coefficient / $W{\cdot}m^{-2}{\cdot}K^{-1}$	Pressure drop / Pa	Working flow rate / $m^3{\cdot}s^{-1}$
H12-basic	$h = 7.99588 + 21.85416q_v - 0.64723q_v^2$ $q_v \in (0.65, 4.63)\ m^3{\cdot}s^{-1}$	$\Delta p = -2.74167 + 10.37656q_v + 14.57428q_v^2$ $q_v \in (0.65, 4.63)\ m^3{\cdot}s^{-1}$	0.65–4.63
H12R10h2	$h = 8.56689 + 32.10129q_v - 1.04129q_v^2$ $q_v \in (0.65, 4.63)\ m^3{\cdot}s^{-1}$	$\Delta p = -6.88863 + 17.45768q_v + 23.57976q_v^2$ $q_v \in (0.65, 4.63)\ m^3{\cdot}s^{-1}$	0.65–4.63
H12R10h3	$h = 15.31114 + 35.13173q_v - 1.20382q_v^2$ $q_v \in (0.65, 4.63)\ m^3{\cdot}s^{-1}$	$\Delta p = -8.63198 + 25.72581q_v + 30.93166q_v^2$ $q_v \in (0.65, 4.63)\ m^3{\cdot}s^{-1}$	0.65–4.63
H12R10h4	$h = 16.72211 + 46.19792q_v - 2.35325q_v^2$ $q_v \in (0.65, 4.63)\ m^3{\cdot}s^{-1}$	$\Delta p = -28.7783 + 57.40514q_v + 41.10834q_v^2$ $q_v \in (0.65, 4.63)\ m^3{\cdot}s^{-1}$	0.65–4.63
H10-basic	$h = 9.15559 + 21.79471q_v - 0.57014q_v^2$ $q_v \in (0.79, 5.58)\ m^3{\cdot}s^{-1}$	$\Delta p = -5.20566 + 15.27683q_v + 15.02503q_v^2$ $q_v \in (0.79, 5.88)\ m^3{\cdot}s^{-1}$	0.79–5.58
H10R10h2	$h = 10.06385 + 31.61734q_v - 0.96364q_v^2$ $q_v \in (0.79, 5.58)\ m^3{\cdot}s^{-1}$	$\Delta p = -11.36523 + 24.68892q_v + 25.72717q_v^2$ $q_v \in (0.79, 5.88)\ m^3{\cdot}s^{-1}$	0.79–5.58
H10R10h3	$h = 16.11953 + 36.40655q_v - 1.19433q_v^2$ $q_v \in (0.79, 5.58)\ m^3{\cdot}s^{-1}$	$\Delta p = -19.77463 + 41.26308q_v + 34.54889q_v^2$ $q_v \in (0.79, 5.88)\ m^3{\cdot}s^{-1}$	0.79–5.58
H10R10h4	$h = 20.84478 + 40.34375q_v - 1.07592q_v^2$ $q_v \in (0.79, 5.58)\ m^3{\cdot}s^{-1}$	$\Delta p = -14.80999 + 38.83369q_v + 55.49611q_v^2$ $q_v \in (0.79, 5.88)\ m^3{\cdot}s^{-1}$	0.79–5.58
H7.5-basic	$h = 11.27382 + 21.76315q_v - 0.46199q_v^2$ $q_v \in (1.06, 7.50)\ m^3{\cdot}s^{-1}$	$\Delta p = -13.66675 + 27.87337q_v + 16.48178q_v^2$ $q_v \in (1.06, 7.50)\ m^3{\cdot}s^{-1}$	1.06–7.50
H7.5R10h2	$h = 13.17021 + 31.01117q_v - 0.83228q_v^2$ $q_v \in (1.06, 7.50)\ m^3{\cdot}s^{-1}$	$\Delta p = -32.86205 + 50.88239q_v + 28.83943q_v^2$ $q_v \in (1.06, 7.50)\ m^3{\cdot}s^{-1}$	1.06–7.50
H7.5R10h3	$h = 18.61383 + 35.92613q_v - 0.96838q_v^2$ $q_v \in (1.06, 7.50)\ m^3{\cdot}s^{-1}$	$\Delta p = -51.0195 + 75.17742q_v + 41.42869q_v^2$ $q_v \in (1.06, 7.50)\ m^3{\cdot}s^{-1}$	1.06–7.50
H7.5R10h4	$h = 24.01557 + 40.4457q_v - 0.98552q_v^2$ $q_v \in (1.06, 7.50)\ m^3{\cdot}s^{-1}$	$\Delta p = -39.2492 + 75.3272q_v + 67.12078q_v^2$ $q_v \in (1.06, 7.50)\ m^3{\cdot}s^{-1}$	1.06–7.50

Appendix B

The typical water pipe system consists of ten racks and a water pipes system. The pressure drop of the water pipe systems can be calculated from the main pipe water inlet to the main pipe water outlet. The calculation path is: the main pipe inlet to the end rack (the farthest rack) inlet port, the end rack inlet port to the end server inlet port, the end server inlet port to the end server outlet port, the end server outlet port to the end rack outlet port, the end rack outlet port to the main pipe outlet. The non-end racks and servers are treated as parallel branches, which is not considered in the pressure drop calculation. Fig. B-1 gives the pressure drop distribution of the water pipes system, including the pipes at the rack level and room level. The WFR distribution is consistent with the chosen ALCS working condition in the main test. The flow duct width of the main pipe is 30 mm, which is three times the flow duct width of the pipes in the rack. Such an arrangement helps to reduce the water flow velocity of the main pipe.

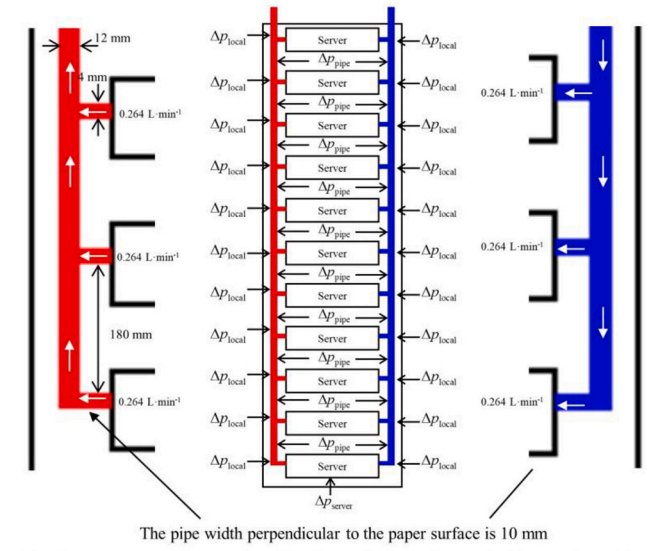

(a) The pressure drops distribution of pipes in rack (the end rack)

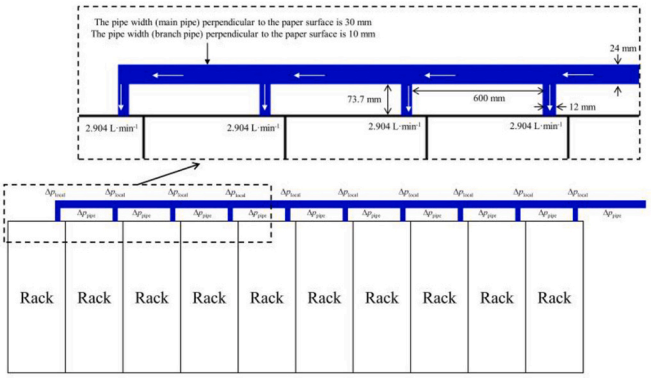

(b) The pressure drop distribution of inlet pipes in room level.

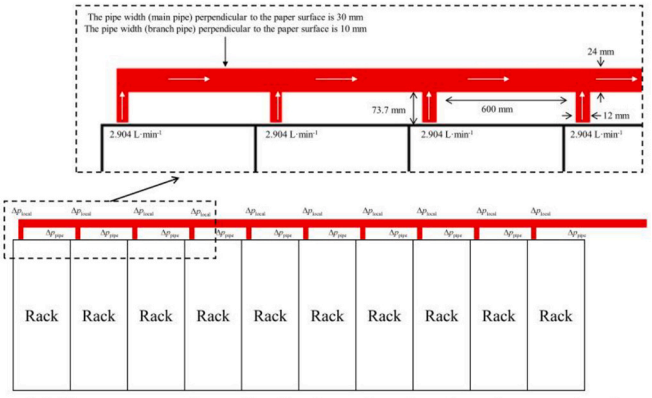

(c) The pressure drop distribution of outlet pipes in room level.

Fig. B-1. The pressure drop distribution of pressure drop in the end rack and the room level. (a) The pressure drops distribution of pipes in rack (the end rack). (b) The pressure drop distribution of inlet pipes in room level. (c) The pressure drop distribution of outlet pipes in room level.

As we can see from Fig. B-1 when the WFRs of the water pipes system are known, the total pressure drop of the water pipes system can be obtained by the sum of local pressure drop Δp_{local} of the bends and wyes (converging and diverging), frictional pressure drop Δp_{pipe} in the long pipes, and the pressure drop of end ALCS Δp_{server}. The Δp_{server} is based on CFD simulation, which is 149.32 Pa under the water volume flow rate shown in Fig. B-1(a). The frictional pressure drop of long pipes Δp_{pipe} can be calculated by:

$$\Delta p_{\text{pipe}} = \lambda \frac{l}{D_h} \frac{\rho u^2}{2} \tag{B-1}$$

where, λ is the frictional coefficient; l is the length of the pipe, m; D_{h} is the hydraulic diameter, m; ρ is water density, 998.2 kg·m^{-3}, u is the water velocity in the pipe, m·s^{-1}.

The frictional coefficient is related to the Reynolds number and calculated by **Eq.(B-2)**.

$$\lambda = \begin{cases} \dfrac{0.3164}{Re^{0.25}} & \text{for } Re > 2300 \\ \dfrac{64}{Re} & \text{for } Re < 2300 \end{cases} \tag{B-2}$$

where, Re is the Reynolds number, calculated by:

$$Re = \frac{\rho u D_h}{\mu} \tag{B-3}$$

where, μ is the dynamic viscosity of water, 0.00101 Pa·s.

Under the chosen ALCSs working condition, the total water volume flow rate is 29.04 L·min^{-1} as shown in Fig. B-1. The WFR in the serial pipes will gradually decrease with the division of local diverging wyes as shown in Fig. B-1(b). Adversely, the WFR in the serial pipes will gradually increase with the merging of local converging wyes as shown in Fig. B-1(c). The long pipe between the adjacent racks has a constant flow rate, and the friction pressure drop in these pipes can be calculated by **Eq.(B-1)**.

The local pressure drop is calculated based on the local structures, which can be divided into three types: bend, converging wye, and diverging wye, as shown in Fig. B-2. The bends are located at the inlet/outlet of the end rack and the inlet/outlet of the end server, while the wyes are located at the inlet/outlet of other racks and servers, as we can see in Fig. B-1. Fig. B-2(a) is the schematic diagram of the local bend, m_1 is the WFR, A_1 and A_2 are respectively the area of the inlet surface and outlet surface. Fig. B-2(b) and Fig. B-2(c) are respectively the schematic diagrams of converging wye and diverging wye. The wyes consist of the main pipe and branch pipe, the inlet and outlet of the main pipe are not changed, and A_{st} is equal to A_c. The local pressure drop of wyes can be calculated by the flow rates and pipe cross-sections as shown in the Fig.

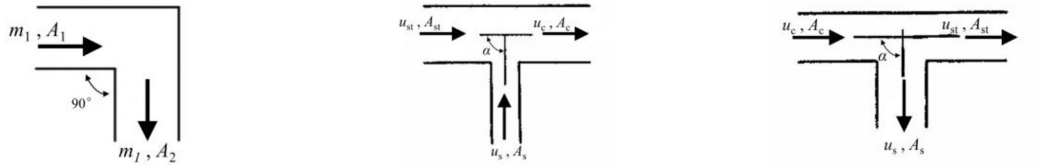

Fig. B-2. The schematic diagram of local bends and wyes. (a) The local bend. (b) The local converging wye. (c) The local diverging wye.

The relationship between the local frictional coefficient and local pressure drop is given in **Eq.(B-4)**:

$$\zeta_e \equiv \frac{\Delta p_{local}}{\rho u_e^2/2} \tag{B-4}$$

where, Δp_{local} is the local pressure drop, Pa; u_e is the inlet velocity of local structure, m·s^{-1}; ζ_e is the.

local frictional coefficient. ζ_e of bends in Fig. B-2(a) is calculated by:

$$\zeta_e = \frac{\Delta p_{local}}{\rho u_1^2/2} = f_{e\text{-}rack}\left(\frac{a}{b}, \frac{A_2}{A_1}\right)$$

$$f_{e-rack}\left(\frac{a}{b}, \frac{A_2}{A_1}\right) = p_{00} + p_{10}\frac{a}{b} + p_{01}\frac{A_2}{A_1} + p_{20}\left(\frac{a}{b}\right)^2 + p_{11}\frac{a}{b}\frac{A_2}{A_1} + p_{02}\left(\frac{A_2}{A_1}\right)^2 + p_{30}\left(\frac{a}{b}\right)^3 + p_{21}\left(\frac{a}{b}\right)^2\frac{A_2}{A_1} + p_{12}\frac{a}{b}\left(\frac{A_2}{A_1}\right)^2 + p_{03}\left(\frac{A_2}{A_1}\right)^3 \tag{B-5}$$

where, a and b are respectively the length and width of the inlet surface, m; A_1 and A_2 are respectively.

the cross-sections area of inlet surface and outlet surface, m^2; u_1 is the velocity of inlet surface, m·s^{-}1; p_{00} to p_{03} is the constant coefficients [40]: p_{00} is 0.8257, p_{10} is −0.1395, p_{01} is −0.1586, p_{20} is 0.07811, p_{11} is −0.01717, p_{02} is 0.1637, p_{30} is −0.04289, p_{21} is −0.004508, p_{12} is 0.01079, p_{03} is −0.06378.

The local pressure drop of the converging wye shown in Fig. B-2(b) is calculated by **Eq.(B-6)** [39].

$$\zeta_{st\text{-}con} = \frac{\Delta p_{st\text{-}con}}{\rho u_c^2/2} = \frac{1.55\frac{q_{v\text{-}s}}{q_{v\text{-}c}} - \left(\frac{q_{v\text{-}s}}{q_{v\text{-}c}}\right)^2}{(u_{st}/u_c)^2} \tag{B-6}$$

where, $\zeta_{st\text{-}con}$ is the local frictional coefficient of converging wye; $\Delta p_{st\text{-}con}$ is the local pressure drop of converging wye, Pa; $q_{v\text{-}s}$ is the bench flow rate of converging wye, m^3·s^{-1}; $q_{v\text{-}c}$ is the main pipe flow rate after converging, m^3·s^{-1}; u_c is the main pipe flow rate after converging, m·s^{-1}; u_{st} is the main pipe flow rate before converging, m·s^{-1}.

The local pressure drop of diverging shown in Fig. B-2(c) is calculated by **Eq.(B-7)** [39]:

$$\zeta_{st\text{-}div} = \frac{\Delta p_{st\text{-}div}}{\rho u_{st}^2/2} = \frac{\zeta_{c.st\text{-}div}}{(u_{st}/u_c)^2} = \frac{\zeta_{c.st\text{-}div}}{(1 - q_{v\text{-}s}/q_{v-c})^2 (A_c/A_{st})^2}$$

$$\zeta_{c.st-div} = 0.406 + 7.72654\left(\frac{q_{v-st}}{q_{v-c}}\right) - 72.45875\left(\frac{q_{v-st}}{q_{v-c}}\right)^2 + 306.55248\left(\frac{q_{v-st}}{q_{v-c}}\right)^3 - 687.45789\left(\frac{q_{v-st}}{q_{v-c}}\right)^4 + 837.92484\left(\frac{q_{v-st}}{q_{v-c}}\right)^5 - 522.71242\left(\frac{q_{v-st}}{q_{v-c}}\right)^6 + 130.71895\left(\frac{q_{v-st}}{q_{v-c}}\right)^7 \quad \text{(B-7)}$$

where, $\zeta_{st\text{-}div}$ is the local frictional coefficient of diverging wye; $\Delta p_{st\text{-}div}$ is the local pressure drop of diverging wye, Pa.

The local pressure drop and frictional pressure drop shown in Fig. B-1 are calculated by the above equations. Under the WFR of the chosen condition in the main test, the pressure drop distribution is shown in Fig. B-3. By summing up the local pressure drop and frictional pressure drop along the water flow direction, a total pressure drop of 2813.42 Pa is obtained for the studied water pipes system in the Fig. The water pipes system only includes the pipes near the racks, while the additional connecting pipes are needed in the real data center to connect the pumps and the water pipe system. The detailed length of additional pipes depends on the racks and pump arrangement in the data center. For every water pipes system in this paper, it is assumed that the length of the water pipes is 12 m. The pressure drop of the additional pipes is obtained as 2778.51 Pa based on **Eq.(B-1)**. Thus, the total pressure drop of the water pipes system in the IT room side is 5591.93 Pa, which is the sum of the pressure drop of a typical water pipes system and additional connecting pipes. The pressure drop of the room-side pump is also 5591.93 Pa (the same as the pressure drop of the room-side water pipes system), which will be further adopted for the pumping power consumption in the main text.

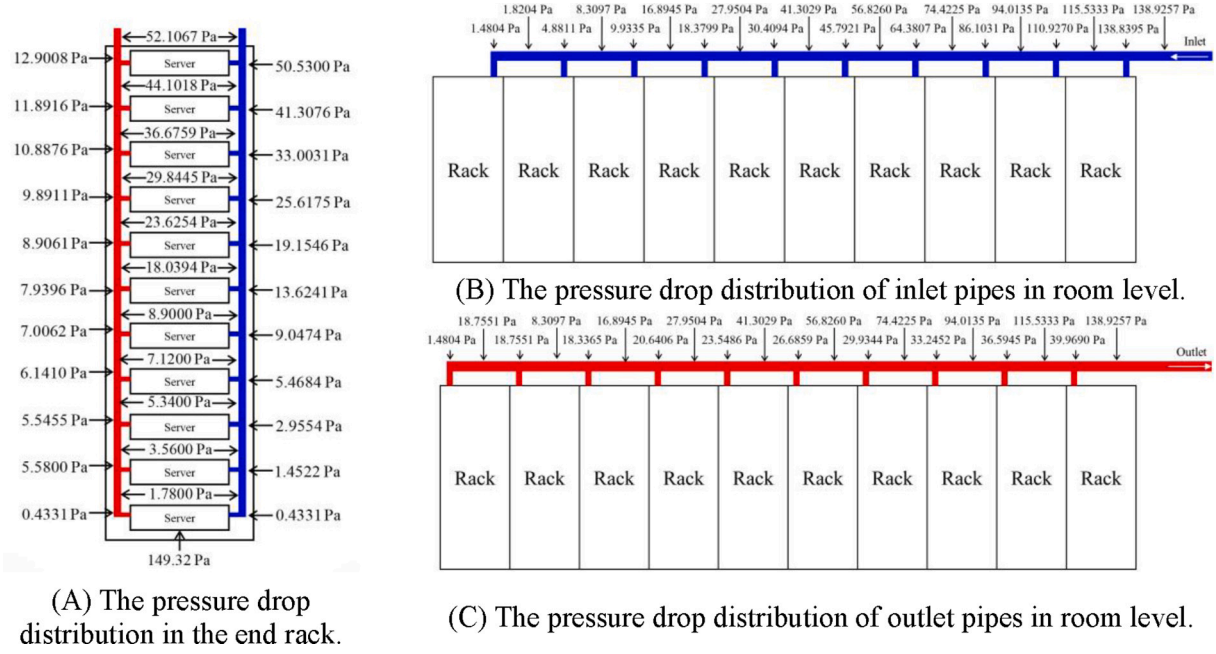

Fig. B-3. The calculation results of pressure drop distribution under the chosen ALCS WFR. (A) The pressure drop distribution in the end rack. (B) The pressure drop distribution of inlet pipes in room level. (C) The pressure drop distribution of outlet pipes in room level.

Appendix C

HTRI Xchanger Suit is used to obtain a reliable MPHE design result for the studied DC unit. The design results are given as follows:
Plate type: manufacturer is Alfa Laval; plate ID is M10-M; chevron angle is 30 degrees; port diameter is 100 mm.
Pack arrangement: single pass and 14 channels per pass for both the hot side and cold side.
Hot side is U arrangement, Cold side is U arrangement.
The process condition of MPHE is given in Table C-1. The MPME exchanger performance is given in Table C-2.

Table C-1
Process condition of the MPHE.

Process condition	Hot side	cold side
Fluid name	Sever cooling water	Cold chilled water
Total flow rate ($kg{\cdot}s^{-1}$)	3.865	22.395
Temperature: inlet / outlet (°C)	74.05 / 44.98	10.00 / 15.01
Temperature: average / skin (°C)	59.51 / 33.93	12.50 / 21.97
Pressure: inlet / average (kPa)	300 / 299.26	300 / 280.45
Pressure drop: total / allow (kPa)	1.487 / 100.00	39.099 / 200.00
Nominal channel velocity ($m{\cdot}s^{-1}$)	0.21	1.18
Fouling resistance ($m^2{\cdot}K{\cdot}W^{-1}$)	3.00e-5	3.00e-5
Equivalent shear stress (Pa)	2.93	82.27
Maldistribution parameter	0.14	0.17

Table C-2
Exchanger performance of MPHE.

Parameter	Value	Parameter	Value
Hot film coefficient ($W \cdot m^{-2} \cdot K^{-1}$)	4189.0	Actual U ($W \cdot m^{-2} \cdot K^{-1}$)	2318.242
Cold film coefficient ($W \cdot m^{-2} \cdot K^{-1}$)	10,571	Required U ($W \cdot m^{-2} \cdot K^{-1}$)	1697.896
EMTD (°C)	45.9	Total duty (kW)	470
Area (m^2)	6.020	Overdesign (%)	36.54

Fig. C-1 is the drawing of MPHE design result.

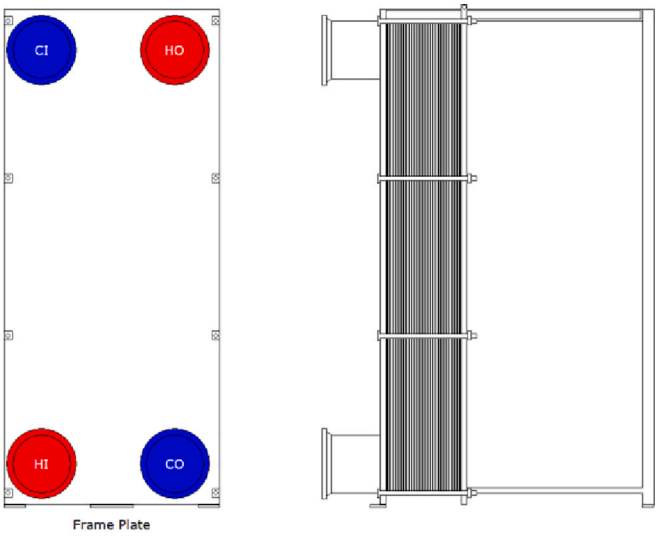

Stream ID	Hotside		Coldside	
Stream name	Hot water		Cold water	
Flow (total), kg/s	3.8650		22.3946	
Pressure drop, kPa	1.487		39.099	
Temperature, C	74.05	44.98	10.00	15.01
Wt. fraction vapor	0.00000	0.00000	0.00000	0.00000
Pressure, kPa	300.000	298.513	300.000	260.901

Fig. C-1. The drawing of the MPHE design result.

Appendix D

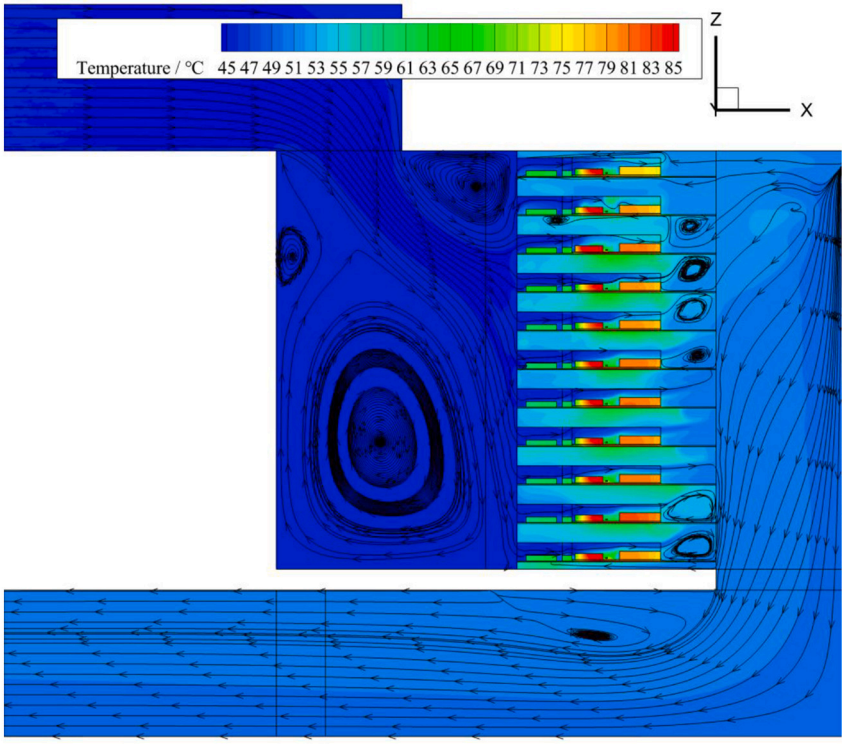

(a) temperature contour and streamline at the cross-section of the IT room when FRS is 500 rad·s^{-1}

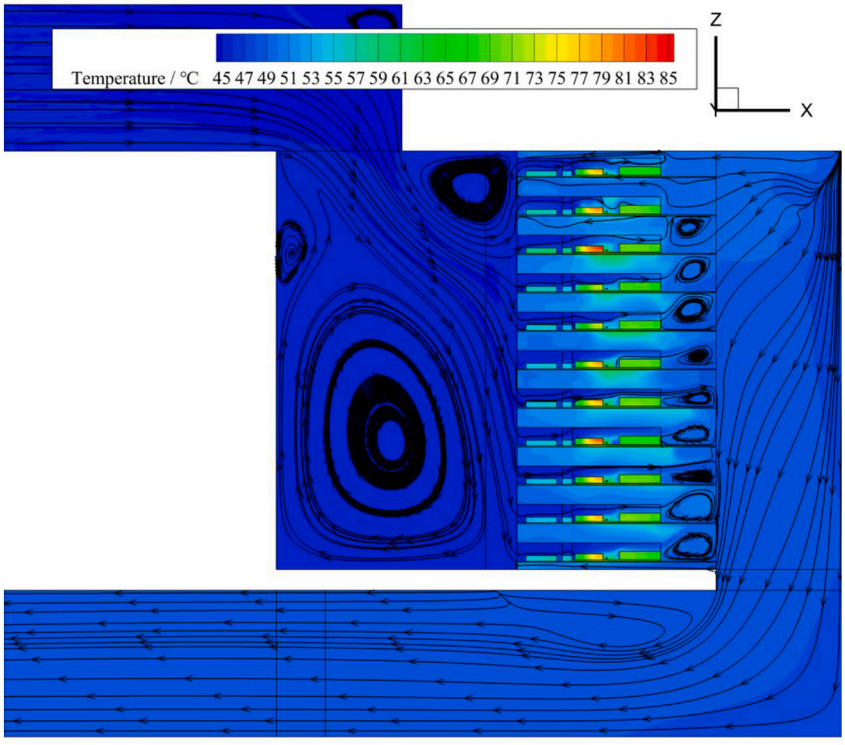

(b) temperature contour and streamline at the cross-section of the IT room when FRS is 850 rad·s^{-1}

Fig. D-1. The streamlines and temperature contours at the cross-section of the IT room and the 3D streamlines in the IT room under different FRS. (a) temperature contour and streamline at the cross-section of the IT room when FRS is 500 rad·s^{-1}. (b) temperature contour and streamline at the cross-section of the IT room when FRS is 850 rad·s^{-1}. (c) temperature contour and streamline at the cross-section of the IT room when FRS is 1000 rad·s^{-1}. (d) 3D streamlines in the IT room when FRS is 500 rad·s^{-1}. (e) 3D streamlines in the IT room when FRS is 850 rad·s^{-1}. (f) 3D streamlines in the IT room when FRS is 1000 rad·s^{-1}.

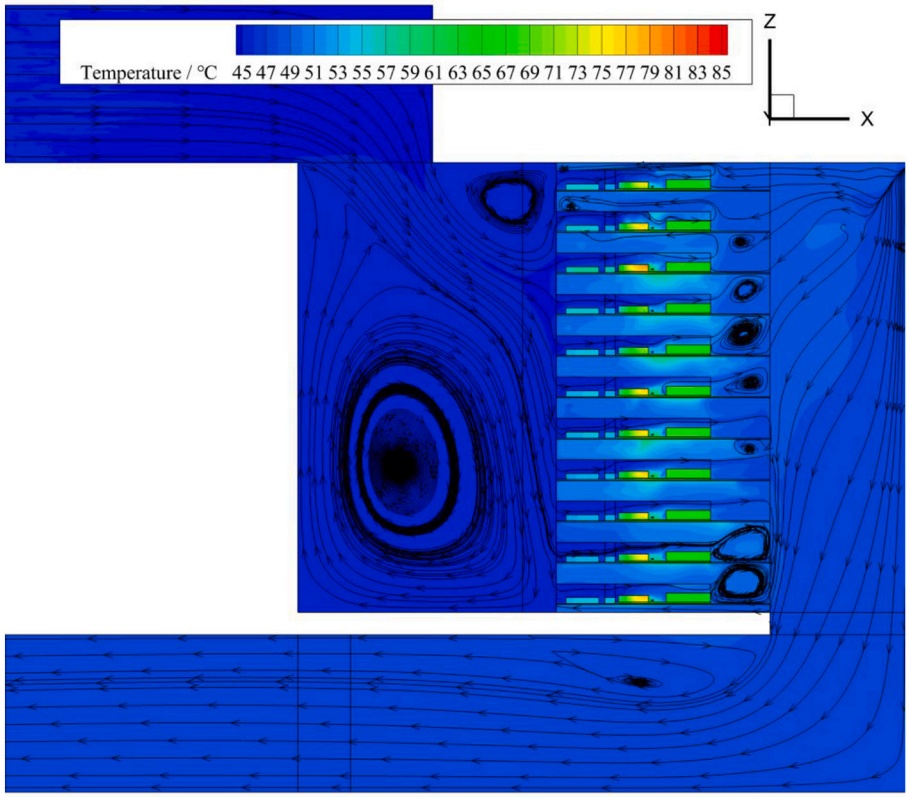

(c) temperature contour and streamline at the cross-section of the IT room when FRS is 1000 rad·s^{-1}

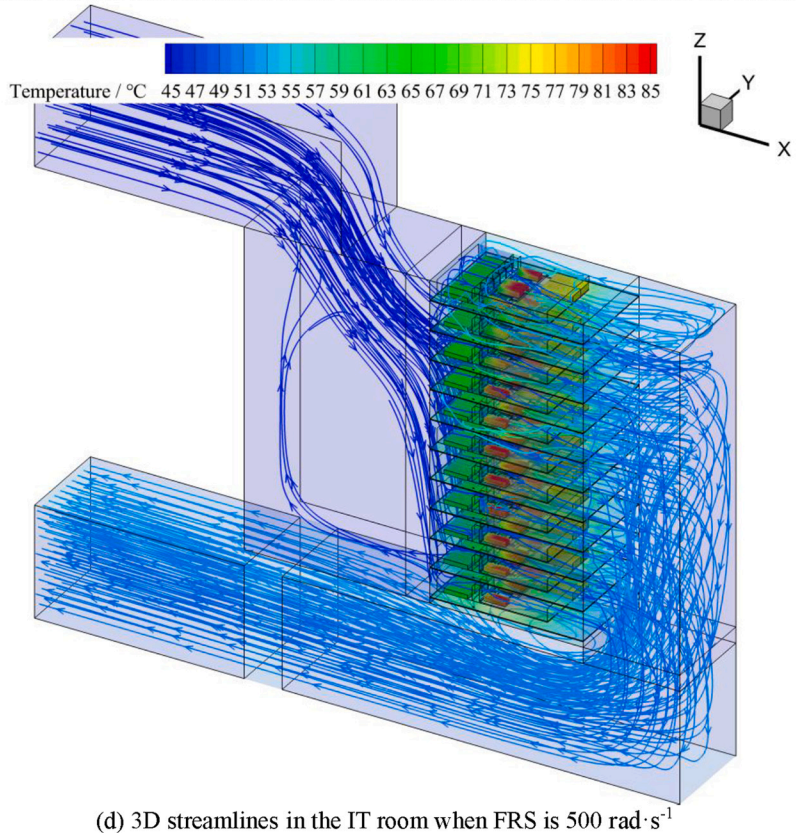

(d) 3D streamlines in the IT room when FRS is 500 rad·s^{-1}

Fig. D-1. (*continued*).

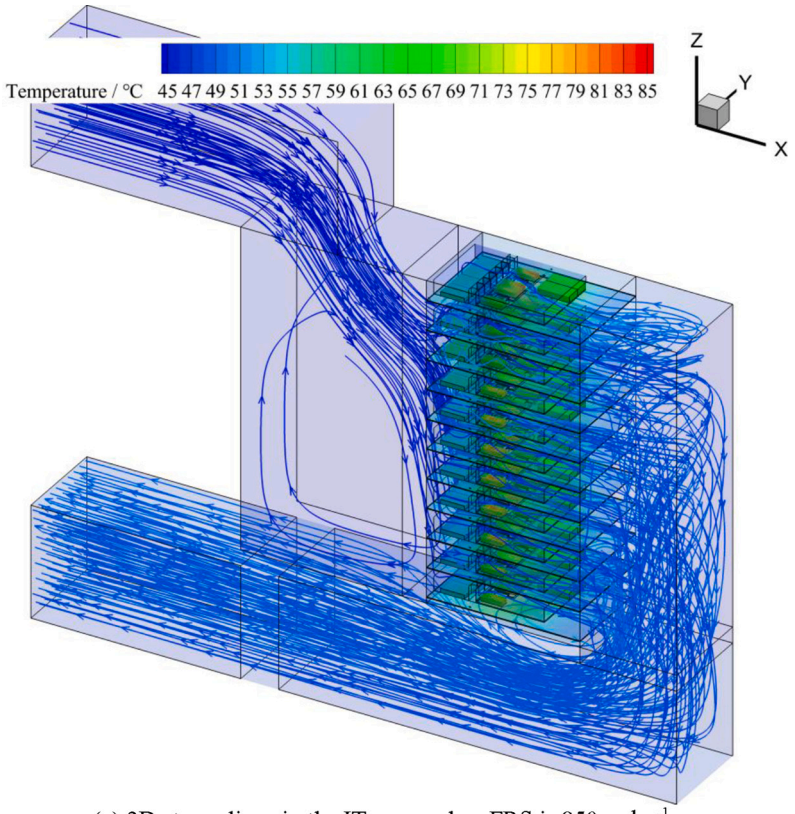

(e) 3D streamlines in the IT room when FRS is 850 rad·s^{-1}

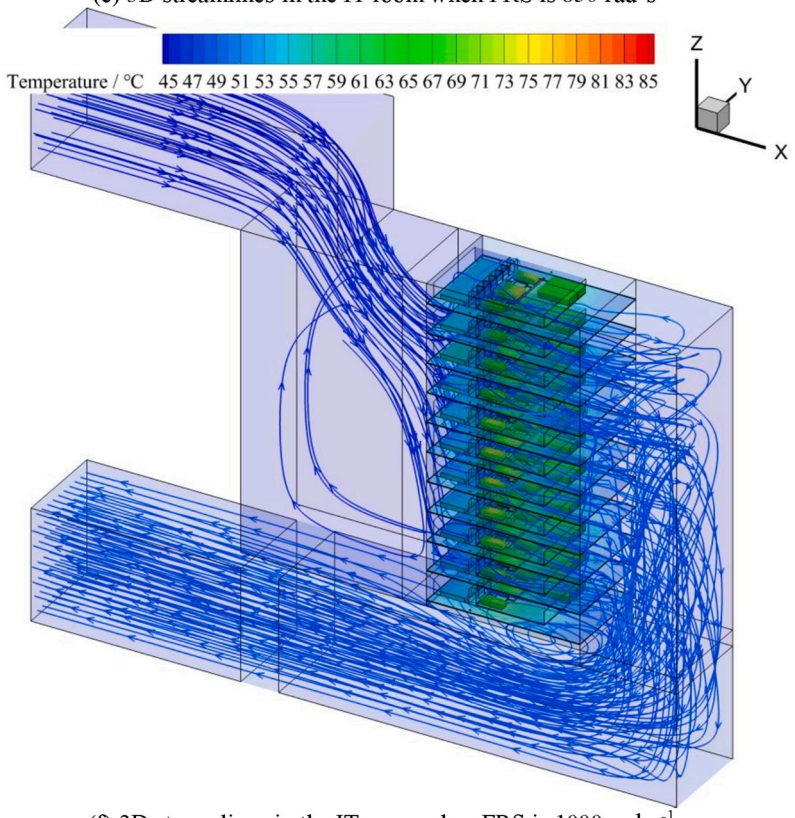

(f) 3D streamlines in the IT room when FRS is 1000 rad·s^{-1}

Fig. D-1. (*continued*).

Appendix E

For the fitted chiller *COP* formula, the $COP_{chiller}$ versus cooling capacity under different environment temperatures and constant return water temperature is given in Fig.E-1.

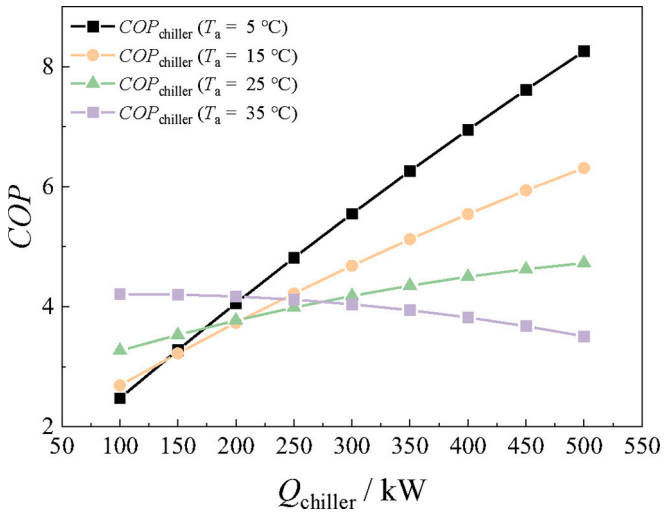

Fig. E-1. $COP_{chiller}$ versus cooling capacity under different Ta (constant Teo = 10 °C)

Appendix F. Supplementary data

Supplementary data to this article can be found online at https://doi.org/10.1016/j.apenergy.2025.127154.

Data availability

Data will be made available on request.

References

[1] IEA. Tracking Data Centres and Data Transmission Networks[OL]. https://www.iea.org/energy-system/buildings/data-centres-and-data-transmission-networks;; 2024. accessed September 12, 2024.

[2] Isazadeh Amin, Ziviani Davide, Claridge David E. Global trends, performance metrics, and energy reduction measures in datacom facilities. Renew Sust Energ Rev 2023;174:113149.

[3] Isazadeh Amin, Ziviani Davide, Claridge David E. Thermal management in legacy air-cooled data centers: an overview and perspectives. Renew Sust Energ Rev 2023;187:113707.

[4] Khalaj Ali Habibi, Abdulla Khalid, Halgamuge Saman K. Towards the stand-alone operation of data centers with free cooling and optimally sized hybrid renewable power generation and energy storage. Renew Sust Energ Rev 2018;93:451–72.

[5] Li Nan, Li Haowei, Duan Kaiwen, et al. Evaluation of the cooling effectiveness of air-cooled data centers by energy diagram. Appl Energy 2025;382:125215.

[6] Khalaj Ali Habibi, Halgamuge Saman K. A review on efficient thermal management of air- and liquid-cooled data centers: from chip to the cooling system. Appl Energy 2017;205:1165–88.

[7] Fulpagare Yogesh, Hsu Po-hao, Wang Chi-chuan. Experimental analysis of airflow uniformity and energy consumption in data centers. Appl Therm Eng 2022;209:118302.

[8] Azarifar Mohammad, Arik Mehmet, Chang Je-young. Liquid cooling of data centers: a necessity facing challenges. Appl Therm Eng 2024;247:123112.

[9] Akeiber Hussein, Nejat Payam, Majid Muhd Zaimi Abd, et al. A review on phase change material (PCM) for sustainable passive cooling in building envelopes. Renew Sust Energ Rev 2016;60:1470–97.

[10] Kong Rui, Zhang Hainan, Tang Mingsheng, et al. Enhancing data center cooling efficiency and ability: a comprehensive review of direct liquid cooling technologies. Energy 2024;308:132846.

[11] Tang Kai, Lin Guiping, Huang Jinyin, et al. Startup categories of manifold microchannel heat sink heated by thermal test chip. Int J Heat Mass Transf 2024;232:125949.

[12] Li Ziyong, Luo Hailiang, Jiang Yuguang, et al. Comprehensive review and future prospects on chip-scale thermal management: Core of data center's thermal management. Appl Therm Eng 2024;251:123612.

[13] Memon Safi Ahmed, Akhtar Shehnaz, Cheema Taqi Ahmad, et al. Enhancing heat transfer in microchannels: a systematic evaluation of crescent-like fin and wall geometries with secondary flow. Appl Therm Eng 2024;239:122099.

[14] Li Yu-Ting, Jin Shu-Qi, Xiao-Jun Hu, et al. Examining performance of microchannel cold plate heat sink from its three parts along coolant flow direction and new structure designs based on the new considerations. Appl Therm Eng 2025;269:125963.

[15] Wang Zi-Xing, Tao Wen-Quan. Heat transfer and pressure drop characteristics of microchannel cold plate in commercial CPU-package cooling system. Int J Heat Mass Transf 2025;246:127060.

[16] Alissa Husam, Nick Teresa, Raniwala Ashish, et al. Using life cycle assessment to drive innovation for sustainable cool clouds. Nature 2025;641:331–8.

[17] Zhang Jifang, He Wei, Guo Rui, et al. Optimal thermal management on server cooling system to achieve minimal energy consumption based on air-cooled chiller. Energy Rep 2022;8:154–61.

[18] Cheung Howard, Wang Shengwei. Reliability and availability assessment and enhancement of water-cooled multi-chiller cooling systems for data centers. Reliab Eng Syst Saf 2019;191:106573.

[19] Zhao Ce, Jing Yang, Xie Xiaoyun, et al. Application and simulation of IEC water chillers for summer free cooling in data centers. Appl Therm Eng 2025;260:124915.

[20] Zhang Hainan, Shao Shuangquan, Hongbo Xu, et al. Free cooling of data centers: a review. Renew Sust Energ Rev 2014;35:171–82.

[21] Daraghmeh Hafizm, Wang Chi-chuan. A review of current status of free cooling in datacenters. Appl Therm Eng 2017;114:1224–39.

[22] Jia Lizhi, Liu Junjie, Wei Shen, et al. Study on the performance of two water-side free cooling methods in a semiconductor manufacturing factory. Energ Buildings 2021;243:110977.

[23] Zhou Yongcheng, Li Shuangxiu, Li Qiang, et al. Energy savings in direct air-side free cooling data centers: a cross-system modeling and optimization framework. Energ Buildings 2024;308:114003.

[24] Shehabi Arman, Horvath Arpad, Tschudi William, et al. Particle concentrations in data centers. Atmos Environ 2008;42:5978–90.

[25] Yang Hongxing, Shi Wenchao, Chen Yi, et al. Research development of indirect evaporative cooling technology: an updated review. Renew Sust Energ Rev 2021;145:111082.

[26] Wang Zi-Xing, Lei Le, Li Nan, et al. Heat transfer performance improvement of air-cooling unit in data center by numerical simulation. J Eng Thermophys 2021;42:3249–53.

[27] Wang Zixing, Ding Hao, Lei Le, et al. Numerical simulation on the flow and heat transfer characteristics in dimple/protrusion enhanced air handling unit in data center. International Communications in Heat and Mass Transfer 2024;157:107710.

[28] Rashidi Saman, Hormozi Faramarz, Sundén Bengt, et al. Energy saving in thermal energy systems using dimpled surface technology – a review on mechanisms and applications. Appl Energy 2019;250:1491–547.

[29] Wang Zixing, Ding Hao, Lei Le, et al. Designing air handling unit in data center and estimating its performance. Int J Heat Mass Transf 2023;213:124340.

[30] ASHRAE Technical Committee (TC). 9.9 thermal guidelines for data processing environments. 5th ed. American Society of Heating, Refrigerating and Air-Conditioning Engineers; 2021.
[31] Steve Strutt. Data Center Efficiency and IT Equipment Reliability at Wider Operating Temperature and Humidity Ranges [R/OL] [2025-06-09], https://www.thegreengrid.org/en/resources/library-and-tools/383-WP%2350—Data-Center-Efficiency-and-IT-Equipment-Reliability-at-Wider-Operating-Temperature-and-Humidity-Ranges; 2012.
[32] Zhang Yingbo, Shan Kui, Li Xiuming, et al. Research and technologies for next-generation high-temperature data centers – state-of-the-arts and future perspectives. Renew Sust Energ Rev 2023;171:112991.
[33] Zhang Yingbo, Li Hangxin, Wang Shengwei. The global energy impact of raising the space temperature for high-temperature data centers. Cell Rep Phys Sci 2023;4:101624.
[34] Iyengar Madhusudan, David Milnes, Parida Pritish, et al. Server liquid cooling with chiller-less data center design to enable significant energy savings. In: 2012 28th annual IEEE semiconductor thermal measurement and management symposium (SEMI-THERM); 2012. p. 212–23. San Jose, CA, USA.
[35] Fan Chengliang, Zou Binwei, Liao Yundan, et al. Evaluation of energy performance and ecological benefit of free-cooling system for data centers in worldwide climates. Sustain Cities Soc 2024;108:105509.
[36] Liao Yundan, Liao Fei, Huang Gongsheng, et al. Investigating the impact of operating parameters on the energy efficiency of evaporative precooling systems in data centers in hot and humid climates. Journal of Building Engineering 2025;104:112353.
[37] Wang Zi-Xing, Tao Wen-Quan. Numerical study on an air-cooling and liquid-cooling combined server for high-temperature data center application. Appl Therm Eng 2025;280:128111.
[38] Lee Yee-ting, Wen Chih-yung, Shih Yang-cheng, et al. Numerical and experimental investigations on thermal management for data center with cold aisle containment configuration. Appl Energy 2022;307:118213.
[39] Idelchik IE. Handbook of hydraulic resistance[M]. 4th revised and augmented ed. New York: Begell House, Inc; 2007.
[40] Yang Zirong, Jiao Kui, Liu Zhi, et al. Investigation of performance heterogeneity of PEMFC stack based on 1+1D and flow distribution models. Energy Convers Manag 2020;207:112502.
[41] Heat transfer research, Lnc. Xchanger Suite. Avaliable at, https://www.htri.net/; 2025.
[42] Ssembatya Martin, Baltazar Juan-carlos, Claridge David E. Evaluating inverse modeling methods for measurement and verification of chiller energy efficiency measures. Appl Energy 2025;378:124805.
[43] Zhao Jing, Chen Ziyi, Li Haonan, et al. A model predictive control for a multi-chiller system in data center considering whole system energy conservation. Energ Buildings 2024;324:114919.
[44] Photovoltaic geographical information system (PVGIS). [OL]. https://re.jrc.ec.europa.eu/pvg_tools/en/; 2022.
[45] Zhang Yingbo, Li Hangxin, Wang Shengwei. Energy performance analysis of multi-chiller cooling systems for data centers concerning progressive loading throughout the lifecycle under typical climates. Build Simul 2024;17:1693–708.